iScience

CellPress
OPEN ACCESS

Article

Mitochondria hormesis delays aging and associated diseases in *Caenorhabditis elegans* impacting on key ferroptosis players

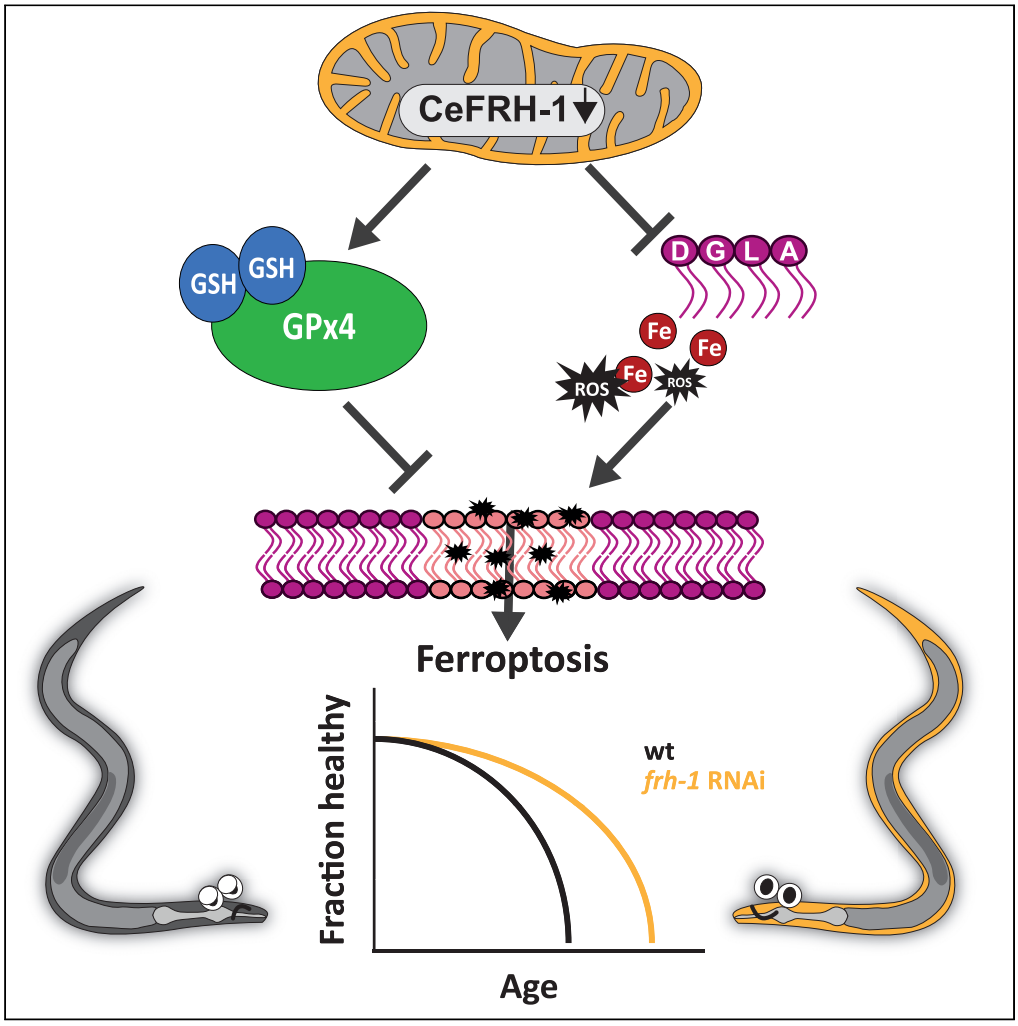

Alfonso Schiavi, Eva Salveridou, Vanessa Brinkmann, ..., Ståle Nygård, Hilde Nilsen, Natascia Ventura

natascia.ventura@uni-duesseldorf.de

Highlights

Sub-lethal iron depletion prevents neuromuscular damage in *C. elegans*

Pro-longevity *frh-1* RNAi counteracts different key ferroptosis players

frh-1 RNAi extends life span via *gpx*-independent, redox, and lipid-regulated systems

frh-1 RNAi protects against hypoxia- and age-induced neuromuscular deficits

Schiavi et al., iScience *26*, 106448
April 21, 2023
https://doi.org/10.1016/j.isci.2023.106448

iScience

CellPress
OPEN ACCESS

Article

Mitochondria hormesis delays aging and associated diseases in *Caenorhabditis elegans* impacting on key ferroptosis players

Alfonso Schiavi,[1] Eva Salveridou,[1,6] Vanessa Brinkmann,[1] Anjumara Shaik,[1,7] Ralph Menzel,[2] Sumana Kalyanasundaram,[3] Ståle Nygård,[5] Hilde Nilsen,[3] and Natascia Ventura[1,4,8,*]

SUMMARY

Excessive iron accumulation or deficiency leads to a variety of pathologies in humans and developmental arrest in the nematode *Caenorhabditis elegans*. Instead, sub-lethal iron depletion extends *C. elegans* lifespan. Hypoxia preconditioning protects against severe hypoxia-induced neuromuscular damage across species but it has low feasible application. In this study, we assessed the potential beneficial effects of genetic and chemical interventions acting via mild iron instead of oxygen depletion. We show that limiting iron availability in *C. elegans* through frataxin silencing or the iron chelator bipyridine, similar to hypoxia preconditioning, protects against hypoxia-, age-, and proteotoxicity-induced neuromuscular deficits. Mechanistically, our data suggest that the beneficial effects elicited by frataxin silencing are in part mediated by counteracting ferroptosis, a form of non-apoptotic cell death mediated by iron-induced lipid peroxidation. This is achieved by impacting on different key ferroptosis players and likely via *gpx*-independent redox systems. We thus point to ferroptosis inhibition as a novel potential strategy to promote healthy aging.

INTRODUCTION

Iron is one of the most abundant components on our planet and it is essential for every living organism on Earth. Iron is indeed necessary as a cofactor for several biological processes, ranging from, just to name some, oxygen transport primarily as a component of hemoglobin,[1] DNA synthesis and repair,[2] mitochondrial respiration,[3] and cell death.[4] It is therefore, not surprising that iron homeostasis must be finely tuned and that either severe iron deprivation or its excessive accumulation has evolutionarily conserved detrimental effects.[5] Interestingly, altered iron homeostasis appears to differentially affect organismal health throughout lifespan. On the one hand iron deficiency is especially detrimental during early development and childhood,[6,7] and its severe deficiency leads to developmental arrest in the nematode *Caenorhabditis elegans* (*C. elegans*).[8] On the other hand, iron excess has primary undesirable effects later in life: its progressive accumulation during aging concurs to the pathogenesis of age-associated neuronal pathologies such as Alzheimer's or Parkinson's diseases, thereby shortening lifespan in the nematode *C. elegans*.[9,10] Aging is a complex biological process characterized by the deterioration of different cellular and organismal structures and functions. Accumulation of iron and of dysfunctional mitochondria are two of the typical hallmarks of aging[11] leading to a vicious cycle that promotes cell and tissue damage, which ultimately contribute to organismal aging.

Similar to iron deficiency also severe mitochondrial dysfunction is primarily associated with neurodevelopmental disorders, such as Friedreich's ataxia (FRDA) or Leigh syndrome.[12] FRDA, is the most frequent inherited recessive ataxia, and it is ascribed to severe deficiency of frataxin; a nuclear encoded mitochondrial protein involved in iron-sulfur-cluster (ISC) proteins biogenesis and iron homeostasis. Accumulation of iron within mitochondria, with consequent alteration of ISC formation and induction of a cytosolic iron-starvation response has been recognized as consequences of frataxin deficiency involved in disease pathogenesis.[13] In line with the disease state, severe or complete frataxin deficiency also induces detrimental effects across species leading to lethality in mice and to developmental arrest in *C. elegans*.[14,15]

Severe hypoxia also has evolutionarily conserved and widely described deleterious consequences, ranging from ischemic stroke and myocardial infarction in mammals to developmental arrest and neuromuscular

[1]Leibniz Research Institute for Environmental Medicine (IUF), Düsseldorf, Germany

[2]Humboldt-Universität zu Berlin, Berlin, Germany

[3]Institute of Clinical Medicine, University of Oslo and Oslo University Hospital, Oslo, Norway

[4]Institute of Clinical Chemistry and Laboratory Diagnostic, Medical Faculty, Heinrich Heine University of Düsseldorf, Düsseldorf, Germany

[5]Bioinformatics Core Facility, Institute for Medical Informatics, Oslo University Hospital, Oslo, Norway

[6]Present address: Department of Psychiatry and Psychotherapy, Medical Faculty, LVR-Klinikum Düsseldorf, Heinrich-Heine-University, Düsseldorf, Germany

[7]Present address: School of Life and Environmental Sciences, University of Sydney, Australia

[8]Lead contact

*Correspondence: natascia.ventura@uni-duesseldorf.de

https://doi.org/10.1016/j.isci.2023.106448

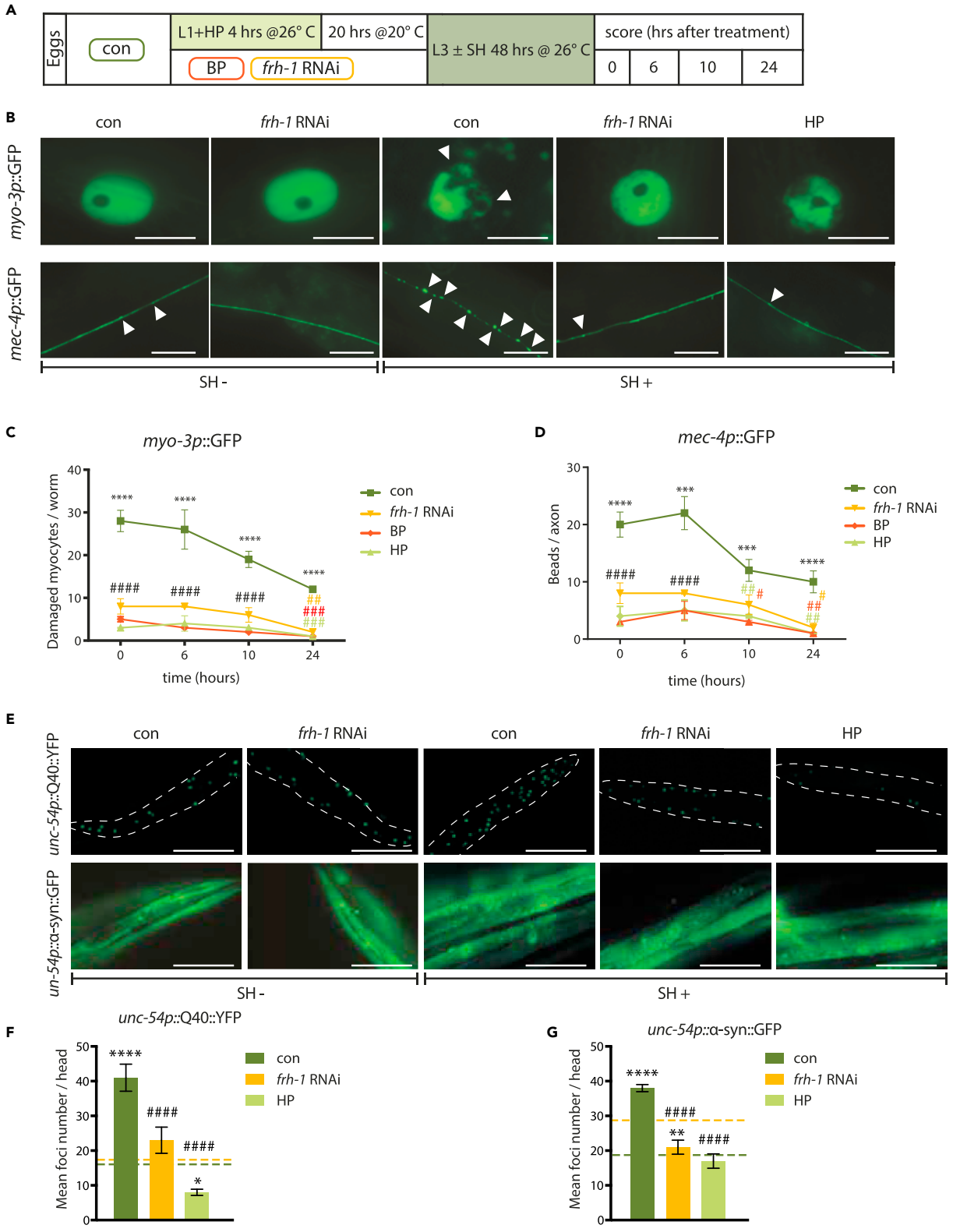
A
Eggs
con
L1+HP 4 hrs @26° C
20 hrs @20° C
BP
frh-1 RNAi
L3 ± SH 48 hrs @ 26° C
score (hrs after treatment)
0
6
10
24
B
con
frh-1 RNAi
con
frh-1 RNAi
HP
myo-3p::GFP
mec-4p::GFP
SH -
SH +
C
myo-3p::GFP
Damaged myocytes / worm
time (hours)
con
frh-1 RNAi
BP
HP
D
mec-4p::GFP
Beads / axon
time (hours)
con
frh-1 RNAi
BP
HP
E
con
frh-1 RNAi
con
frh-1 RNAi
HP
unc-54p::Q40::YFP
un-54p::α-syn::GFP
SH -
SH +
F
unc-54p::Q40::YFP
Mean foci number / head
con
frh-1 RNAi
HP
G
unc-54p::α-syn::GFP
Mean foci number / head
con
frh-1 RNAi
HP

Figure 1. Iron and frataxin depletion protect against hypoxia-induced neuromuscular damage

(A) Schematic representation and pictures of the exposure scenario. Embryos fed bacteria transformed with empty-vector (con) were left untreated or pretreated as L1 with hypoxic preconditioning (HP, i.e., 4 h at 26°C) and left recovering for 20 h before exposure as L3 to severe hypoxia (SH, i.e., 48 h at 26°C). Alternatively, embryos fed bacteria transformed with either empty-vector (con) or vector-expressing dsRNA against *frh-1* (*frh-1* RNAi) or treated with 10 μM of iron chelator 2,2′-dipyridyl (BP), were left untreated or treated with severe hypoxia.

(B) Representative pictures of single nuclear myocytes (*myo-3p*::GFP, upper panels) and single axon (*mec-4p*::GFP, lower panels) of *C. elegans* reporter strains, fed and treated as in (A). SH-, animals left untreated; SH+, animals treated with severe hypoxia. Arrows indicate fragmented myocytes and damaged axon. Pictures were acquired immediately after severe hypoxia treatment. Scale bars are 3.5 μm for *myo-3p*::GFP and 3 μm for *mec-4p*::GFP.

(C and D) Quantification of damaged myocytes per worm in *myo-3*::GFP and of damaged axons in *mec-4*::GFP (C) fed and treated as in (A). Damage was scored after 0, 6, 10, and 24 h after the severe hypoxia treatment. Each time point represents mean ± SEM from n = 3 independent replicas with an average of N = 20 worms; ***p value < 0.001, ****p value < 0.0001 versus control untreated. #p value < 0.05, ##p value < 0.01 ####p value < 0.0001 versus control treated with SH, colors represent the comparison of the corresponding conditions, black hashtags represent the p value of all the conditions (i.e., *frh-1* RNAi, BP, and HP) versus control treated with SH. two-way ANOVA (Tukey's multiple comparison test) E) Representative pictures of *unc-54*p::Q40::YFP (upper panels) and *unc-54p*::a-syn::GFP (bottom panels) *C. elegans* strains, fed and treated as in (A). Images were acquired 24 h after the severe hypoxia treatment. Scale bars are 0.2 mm for *unc-54p*::Q40::YFP and 0.1 mm for *unc-54p*::a-syn::GFP.

(F and G) Quantification of fluorescent foci number in *unc-54*p::Q40::YFP (F) and in *unc-54p*::a-syn::GFP (G) strains, fed and treated as in (E). Foci number were scored 24 h after SH. Bar graphs represent mean ± SEM (n = 2, N = 20); dashed lines represent untreated control (green) and untreated *frh-1* RNAi (yellow). *p value < 0.05, ****p value < 0.0001, versus control untreated (green dashed line), **p value < 0.01 versus *frh-1* RNAi untreated (yellow dashed line), ####p value < 0.0001 versus control treated with SH. two-way ANOVA (Tukey's multiple comparison test.

degeneration in the nematode *C. elegans*.[16,17] However, exposure to non-lethal levels of hypoxia or hypoxia preconditioning (HP) has been shown to prevent the detrimental effects of severe hypoxia-induced neuronal degeneration in an evolutionarily conserved manner.[18,19] Of note, also non-toxic levels of iron depletion achieved with the iron chelator BP or through frataxin (*frh-1*) silencing, extends *C. elegans* lifespan through hypoxia like-induction of mitophagy.[8] While the potential beneficial health effects of HP are obvious, its actual exploitation is hampered by the low feasibility of its practical application. In this study, we thus asked whether non-toxic preconditioning interventions acting on iron instead of oxygen availability may also elicit beneficial responses.

We found that, similar to HP, limiting iron availability at sub-lethal doses through chemical (iron chelators) or genetic (*frh-1* silencing) interventions has protective effects against hypoxia- and age-induced damage. In search of a common mechanistic denominator for the beneficial effects of the iron depleting interventions we sought to investigate the possible impact of ferroptosis, a form of non-apoptotic cell death specifically mediated by iron-induced lipid peroxidation.[20] We found that fatty acids (FA) and glutathione (GSH) homeostasis play a specific role in *frh-1*-control of lifespan, which, along with our previous work, support *frh-1* depletion impacts on different key players of the ferroptosis machinery. Moreover, a combined omics analysis comparing wild-type and *frh-1*-depleted animals throughout life, pointed toward important changes in redox reaction activities and lipid homeostasis, two processes critically involved in ferroptosis. The anti-aging effects of *frh-1* depletion are likely achieved through novel GSH peroxidase (*gpx*)-independent mechanism, which we propose as potential new strategy to delay aging and associated neuromuscular pathologies.

RESULTS

Iron depletion protects against hypoxia-induced neuromuscular damage

In normoxic conditions, the hypoxia-inducible-factor (HIF1α) is hydroxylated by enzymes requiring oxygen, iron, and 2-oxoglutarate. This leads to the subsequent ubiquitination and degradation of HIF1α via the proteasome. Low oxygen and iron concentrations diminish hydroxylase activities and prevent HIF1α degradation in turn promoting its translocation into the nucleus, and its transcriptional modulation of a variety of downstream genes containing hypoxia response elements (HRE).[21,22] Accordingly, iron chelators such as deferoxamine (DFO) or bipyridine (BP), as well as iron competing-metals such as cobalt chloride ($CoCl_2$) or nickel chloride ($NiCl_2$), have been shown to work as hypoxia mimetics by inactivating HIF1 hydroxylases.[23] Opposite to its severe deficiency sub-lethal level of iron depletion extends *C. elegans* lifespan,[8] and we now assessed whether it could—similar to HP—protect against hypoxia-induced neuromuscular damage (Figure 1A). As previously described by others,[18] we observed that severe hypoxia (SH) in the L3 larvae (< 1% O_2 at 26°C for 48h) induces a dramatic accumulation of fragmented nuclei in the muscle of the *myo-3p*::GFP transgenic reporter strain, as well as the characteristic axonal beading in the touch receptor neuron of the *mec-4p*::GFP expressing strain (Figure 1B; Figures 1C and 1D—dark green at t0; Figures S1A and S1B). The SH-induced neuromuscular damage is followed by time-dependent recovery after return to normoxic conditions (Figures 1C and 1D—dark green from 6 to 24 h; Figures S1A and

S1B). Recovery is more or less pronounced likely depending on initial amount of damage, yet being always significant and reproducible in this experimental setting. Moreover, according to the literature,[18] HP in the L1 larvae (< 1% O_2 at 26°C) significantly prevented SH-induced nuclei fragmentation and axonal beading at each of the observed time point (Figure 1B; Figures 1C and 1D—light vs dark green lines; Figures S1A and S1B). Our previous work revealed that mild mitochondrial stress (or mitochondria hormesis), via depletion of the nuclear encoded mitochondrial protein FRH-1, extends lifespan via iron depletion.[8] Strikingly, similar to HP, *frh-1* RNAi significantly prevented SH-induced nuclei fragmentation and axonal beading at each of the observed time point (Figure 1B; Figures 1C and 1D—yellow vs dark green lines; Figures S1A and S1B). To support the beneficial effects of iron-depletion against SH with a chemical intervention, we then took advantage of the iron chelator BP.[8] Of note, similar to *frh-1* RNAi and HP, pro-longevity doses of BP from hatchlings also significantly prevented SH-induced neuromuscular defects at each of the observed time point (Figures 1C and 1D—orange vs dark green lines; Figures S1A–S1C).

As a result of the neuromuscular damage, we expected SH to be accompanied by detrimental effects in different health-related parameters. Indeed, SH significantly reduced animals' fertility (eggs laid in 4 h), locomotion (body bends per minute), and pharyngeal muscle activity (pumping per minute) compared to untreated controls in both *myo-3p*::GFP and *mec-4p*::GFP strains (Figures S1D–S1I—dark green bars vs dark green lines). Of note, the detrimental effects on these parameters were prevented by HP, *frh-1* RNAi, or BP pretreatments (Figures S1D–S1I), although not always completely (Figures S1G and S1H). Thus, reducing iron availability via genetic or chemical interventions mimics the beneficial effects of HP against hypoxia-induced neuromuscular damage.

Pro-longevity frataxin depletion protects against hypoxia- and age-induced proteotoxicity

Excessive iron amount is a widely established mediator of age-associated neurodegenerative disorders (NDD)[5,24] and progressive accumulation and toxicity of aggregation-prone proteins in these diseases is worsened by excessive iron levels.[5] Thus, we wondered whether *frh-1* silencing could also promote beneficial effects in *C. elegans* strains expressing human aggregation-prone proteins, poly-Q40 and α-synuclein (under a muscle specific promoter, *unc-54*), and widely exploited as model systems to respectively study Huntington's and Parkinson's diseases.[25–27] SH in *C. elegans* negatively impacts on protein homeostasis with consequent proteotoxicity.[28] Accordingly, we observed that 48 h hypoxia in the L3 larvae induces a dramatic accumulation of poly-Q40 and α-synuclein aggregates (Figure 1E; Figures 1F and 1G—dark green bars vs dark green lines). Of note, similar to the protective effect provided against neuromuscular damage, HP and *frh-1* RNAi also significantly prevented SH-induced aggregation of these two pathogenetic proteins (Figure 1E; Figure F, G—light green and yellow bars vs dark green bars).

Interestingly, HP and *frh-1* RNAi decreased the amount of SH-induced protein aggregation, i.e., poly-Q40 and α-synuclein respectively, less than in their respective untreated controls (green and yellow lines, respectively), clearly reminiscent of a hormetic effect. In further support of a typical hormetic effect, *frh-1* RNAi in basal conditions already increased the number α-synuclein aggregates (Figure 1E bottom panels; Figure G—yellow line vs dark green line).

In basal conditions, the accumulation of poly-Q40 and α-synuclein aggregates also increases in age-dependent manner (Figures 2A–2D). Remarkably, and in further support of a protective effect against proteotoxicity, we found that *frh-1* RNAi significantly reduced age-dependent accumulation of both poly-Q40 and α-synuclein aggregates (Figures 2A–2D). Moreover, *frh-1* RNAi extended lifespan (Figures 2E and 2F; Table 1) and ameliorated health-related parameters (Figures S2A and S2B) in the two age-associated NDD models. To strengthen the protective role of frataxin depletion against age-associated NDD, we then took advantage of one of the most commonly used *C. elegans* strain to study Alzheimer's disease, which expresses human toxic Aβ under a muscle specific promoter.[29,30] As expected, control animals undergo accelerated time-dependent paralysis induced by Aβ overexpression after temperature upshift and, most notably, *frh-1* RNAi drastically prevented it (Figure S2C). Thus, mitochondria preconditioning achieved through frataxin depletion not only promotes life- and health-span in wild-type animals, but also protects against hypoxia-, age-, and proteotoxic diseases-induced neuromuscular deficits.

DGLA prevents frataxin silencing extension of lifespan

Ferroptosis is a regulated form of non-apoptotic cell death initiated by iron-dependent peroxidation of lipids, especially of FA,[4,20,31] which is emergingly being implicated in the pathogenesis of iron-mediated

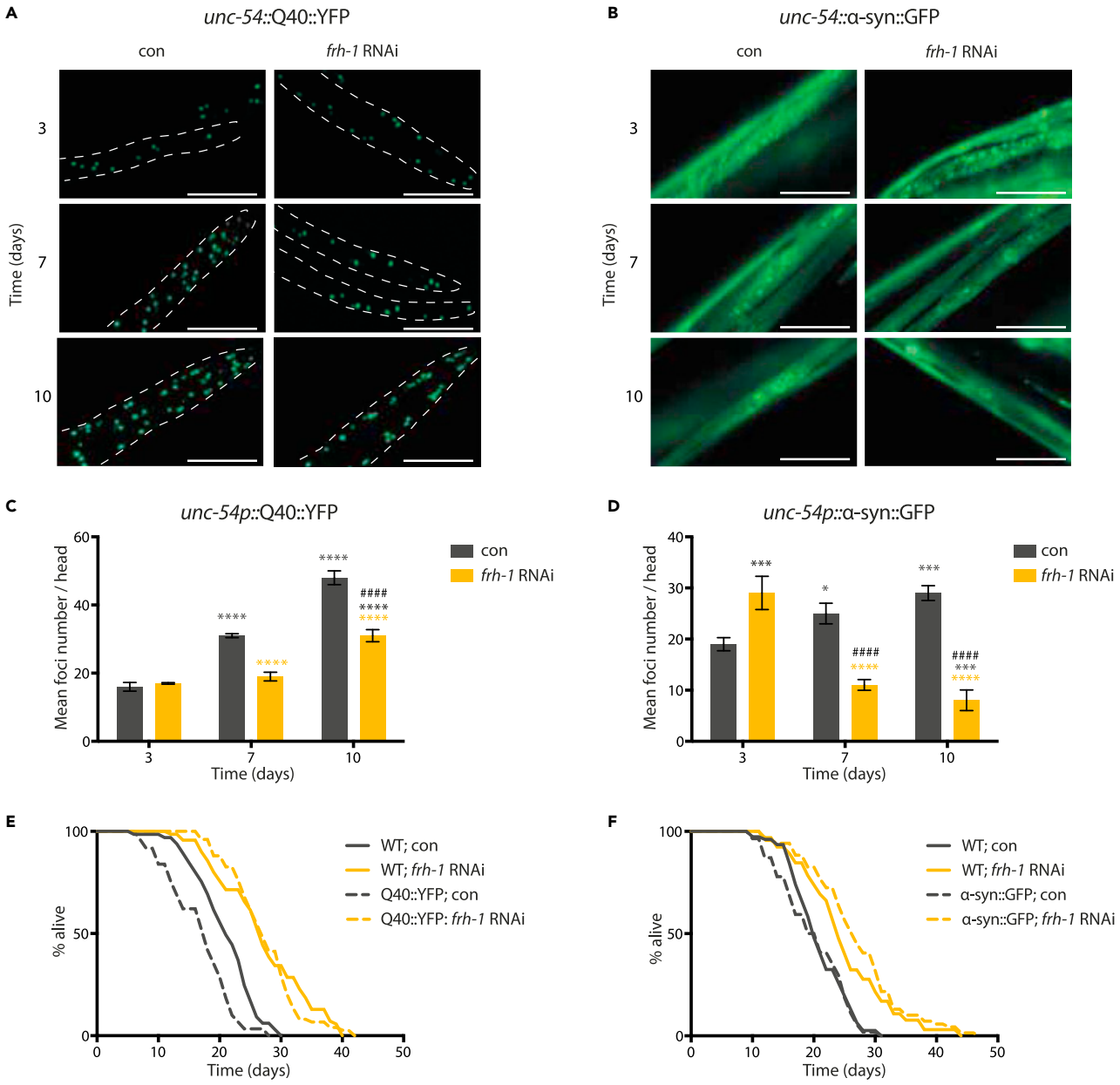

Figure 2. Frataxin depletion protects against hypoxia- and age-induced proteotoxicity

(A and B) Representative pictures of *unc-54p*::Q40::YFP (A) and *unc-54p*::a-syn::GFP (B) reporter strains acquired at 3-, 7-, and 10-day after hatching and fed bacteria transformed with either empty-vector (con) or vector-expressing dsRNA against *frh-1* (*frh-1* RNAi). Scale bars are 0.2 mm for unc-54p::Q40::YFP and 0.1 mm for unc-54p::a-syn::GFP.

(C and D) Quantification of foci number in *unc-54p*::Q40::YFP (C) and *unc-54p*::a-syn::GFP (D) strains in the head region of worms fed and acquire as in (A-B). Bar graph represents mean ± SD (n = 3, N = 20). Black "*" indicate p values versus control (3 days) and yellow "*" versus *frh-1* RNAi (3 days): *p value < 0.05, ***p value < 0.001, ****p value < 0.0001. "#" indicate p values versus control at the same time point: ####p value < 0.0001. two-way ANOVA (Tukey's multiple comparison test) (E-F) Kaplan-Meier survival curves of wild-type (WT) animals, *unc-54*p::Q40::YFP (E), *unc-54p*:a-syn::YFP (NL5901) (F) strains fed as in A. Comparison between curves was done using the log-rank test (Table 1).

NDD.[32,33] In *C. elegans*, frataxin silencing decreases the amount of iron of reactive oxygen species (ROS) and within different metabolic pathways, it specifically reduces the expression of FA metabolism regulatory enzymes (e.g., gpdh-2, lipl-4, acs-17, and fasn-1), as well as the overall animal content of lipids.[8,34] Thus, we wondered whether *frh-1* RNAi, impacting on the two core players of the ferroptosis machinery (i.e., iron and lipid content) may promote life- and health-span ultimately via ferroptosis inhibition. To start assessing this

Table 1. Summary of survival analysis

	Genotype	Treatment	Mean Lifespan (days)	Standard Error	[a]p vs con	[a]p vs WT	Age at 100% mortality (days)	Total/Censor	N
Figure 2E	Wild-type (N2)	PL4440 (con)	22,2	0.4			33	160/20	2
		frh-1 RNAi	26.6	0.6	< 0.0001		42	160/27	2
	AM141 (unc-54p::Q40::YFP)	PL4440 (con)	17.2	0.4		< 0.0001	31	160/47	2
		frh-1 RNAi	27.5	0.6	< 0.0001	ns	45	160/11	2
Figure 2F	Wild-type (N2)	PL4440 (con)	21.3	0.4			33	160/7	2
		frh-1 RNAi	25.4	0.7	< 0.0001		45	160/30	2
	NL5901 (unc-54p::αsyn::YFP)	PL4440 (con)	20.2	0.5		ns	35	160/33	2
		frh-1 RNAi	26.4	0.6	< 0.0001	ns	47	160/35	2
Figure 3H	Wild-type (N2)	PL4440 (con)	19.6	0.5			34	120/14	2
		frh-1 RNAi	22.8	0.8	0.0004		39	120/44	2
		PL4440 DGLA 10μM	19.7	0.5	1		30	120/14	2
		frh-1 RNAi DGLA 10μM	17.2	0.5	0.0055	< 0.0001	34	120/46	2
Figure 3I	Wild-type (N2)	con	20.6	0.3			31	195/9	3
		DGLA 10μM	20.1	0.4	Ns		30	195/13	3
		$CoCl_2$ 500 μM	34.6	0.8	< 0.0001	< 0.0001[b]	50	195/72	3
		CoCl2 500 μM / DGLA 10μM	25.4	0.7	< 0.0001	< 0.0001[b]	37	195/67	3
Figures 4C and 4D	Wild-type (N2)	PL4440 (con)	21.2	0.5			35	140/13	2
		frh-1 RNAi	26.8	0.6	< 0.0001		45	140/20	2
		PL4440 (con) DEM 1.5 mM	12.5	0.2	< 0.0001		17	140/10	2
		frh-1 RNAi DEM 1.5 mM	23.0	0.6	0.0092		40	140/23	2
		PL4440 (con) Lip-1 200 mM	21.4	0.5	Ns		38	140/12	2
	KPJ2 (GPx4)	PL4440 (con)	19.1	0.4		< 0.0001	33	140/12	2
		frh-1 RNAi	24.0	0.7	< 0.0001	ns	45	140/10	2
		PL4440 (con) Lip-1 200 mM	20.7	0.4	Ns	ns	33	138/5	2

(*Continued on next page*)

Table 1. *Continued*

	Genotype	Treatment	Mean Lifespan (days)	Standard Error	[a]p vs con	[a]p vs WT	Age at 100% mortality (days)	Total/Censor	N
Figures S3B and S3C	Wild-type (N2)	PL4440 (con)	19.6	0.5			34	120/14	2
		frh-1 RNAi	22.8	0.8	0.0004		39	120/44	2
		PL4440 OA 10μM	18.6	0.4	Ns		28	120/14	2
		frh-1 RNAi OA 10μM	18.6	0.6	Ns	ns[c]	32	120/51	2
		PL4440 LA 10μM	19.2	0.5	Ns		34	120/11	2
		frh-1 RNAi LA 10μM	18.7	0.6	Ns	ns[d]	36	120/58	2
	Genotype	Treatment	Mean Survival (hours)	Standard Error	[a]p vs con		Age at 100% mortality (hours)	Total/Censor	N
Figure 4B	Wild-type (N2)	con DEM 1.5 mM	31.2	1.1			48	205/51	4
		frh-1 RNAi DEM 1.5 mM	56.2	1.1	< 0.0001		72	194/23	4
		Lip-1 200 mM DEM 1.5 mM	37.1	1.1	0.002		72	199/29	4

[a]Pairwise comparisons using Log-Rank test, P adjusted using the Bonferroni method.
[b]p value vs DGLA 10μM
[c]p value vs PL4440 OA 10μM
[d]p value vs PL4440 LA 10μM

hypothesis, we first carried out a targeted lipidomic analysis in 1-day-old animals left untreated or treated with *frh-1* RNAi and specifically measured the amounts of FA and eicosanoids previously shown to regulate *C. elegans* lifespan and response to hypoxia.[35,36] We found that *frh-1* depletion significantly affects the content of specific FA (Figure 3A) but not that of eicosanoids (Figure S3A). Namely, upon *frh-1* RNAi, the amount of myristoleic acid (MA or 14:1, n-5), oleic acid (OA or 18:1, n-9 *trans*), and linoleic acid (LA or 18:3, n-6) were significantly increased while the content of di-gamma-linoleic acid (DGLA, 20:3, n-6) was significantly decreased. In line with the changes in the FA content, the expression of two critical proteins involved in polyunsaturated fatty acids (PUFA) biosynthesis, FAT-6 and FAT-7 was decreased upon *frh-1* RNAi (Figures 3B and 3C).

PUFA and in particular DGLA, play a critical role in lipid peroxidation-mediated ferroptosis in both mammalian cells and in *C. elegans*.[31] We thus interrogated whether the reduced production of DGLA could be causally involved in the specification of *frh-1* depleted animals' features. To address this, we supplemented DGLA in the worm diet through the entire lifespan in animals left untreated or subjected to *frh-1* RNAi. DGLA supplementation did not affected the expression of typical mitochondrial stress responses genes neither in basal conditions nor upon *frh-1* RNAi (*hsp-6* and *gst-4*, Figures 3D and 3E). This also excluded a non-specific effect of DGLA on the RNAi potency. Instead, DGLA suppressed the small size (Figure 3F), and the reduced fertility (Figure 3G) of *frh-1*-depleted animals, and, most notably, it completely abolished their extended lifespan (Figure 3H; Table 1). DGLA supplementation also partially suppressed the lifespan extension induced by the iron competing agents $CoCl_2$[37] (Figure 3I; Table 1). Interestingly, feeding with other fatty acids, namely OA and LA, whose content was increased by *frh-1* RNAi did not affect lifespan in wild-type but prevented *frh-1* RNAi extension of lifespan (Figures S3B and S3C), supporting a specific role for FA homeostasis in frataxin regulated longevity.

Frataxin depletion extends lifespan via GSH/GPx-dependent and -independent mechanisms

We then sought to investigate the relationship between frataxin depletion and additional key players of the ferroptosis machinery. FA represent a core substrate for iron-induced lipid peroxidation,[38,39] and we thus wondered whether the effects of frataxin silencing on FA imbalance, and especially on DGLA depletion translates into altered lipid peroxidation. We specifically focused on GSH-regulated processes since in *C. elegans*, *frh-1* RNAi also increases the pool of reduced GSH[34] and, in mammals, ferroptosis can be induced by depletion of the GSH-Peroxidase-4 (GPX4), an enzyme which help maintaining appropriate levels of reduced GSH.[40,41] Consistent with the detrimental effect of imbalanced GSH homeostasis, high doses of the GSH-conjugating reagent diethyl-maleate (DEM) have toxic effects in *C. elegans*—in part suppressed by the specific ferroptosis inhibitor liproxstatin (Lip-1)[42] —and shortens animals' lifespan.[43] In line with the pro-ferroptotic role of GSH depletion, acute treatment of *C. elegans* with high doses of the GSH-conjugating reagent diethyl-maleate (DEM), increased lipid peroxidation revealed by the oxidation of the fluorescent FA analog BODIPY-C11 *in vivo* (Figure 4A). Interestingly, pro-longevity *frh-1* RNAi increased probe oxidation to a similar extent, yet prevented DEM-induced lipid peroxidation (Figure 4A), indicative of a typical hormetic effect. To validate the effect of frataxin depletion on lipid peroxidation, we turned to a more classical biochemical approach and measured the production of malondialdehyde (MDA), an end-product of lipid peroxidation reaction.[44,45] Of note, DEM treatment increased the amount of produced MDA and this was also prevented by *frh-1* RNAi, which nonetheless did not per se increased MDA production (Figure S3D).

According to previous findings,[42] we observed that high doses of DEM in *C. elegans* exhibit acute toxicity with 50% of the population dying within 18 h. DEM toxicity was in part suppressed by Lip-1 with 50% of the population still alive after 24h (Figure 4B). Remarkably, we also found that *frh-1* RNAi suppressed acute DEM toxicity much more efficiently than Lip-1 with 50% of the population being still alive after 48h (Figure 4B). Moreover, frataxin depletion significantly rescued the short lifespan induced by chronic supplementation of sub-lethal doses of DEM (Figure 4C; Table 1). Thus, pro-longevity *frh-1* suppression provides protection against acute and chronic GSH depletion, possibly via inhibition of ferroptosis.

To further address the role of ferroptosis in the aging process via genetic rather than chemical interventions, we turned to a *C. elegans* strain with a concurrent deletion of four GPx genes (*gpx-1, -2, -6, -7*, or GPx4), including orthologs of mammalian GPX4, which has been shown to shorten animals lifespan.[46] Notably, consistent with the DEM data, and in further support of anti-ferroptotic effect, *frh-1* RNAi significantly rescued the short lifespan of the GPx4 quadruple mutant (Figure 4D; Table 1). However, the lifespan shortening effects

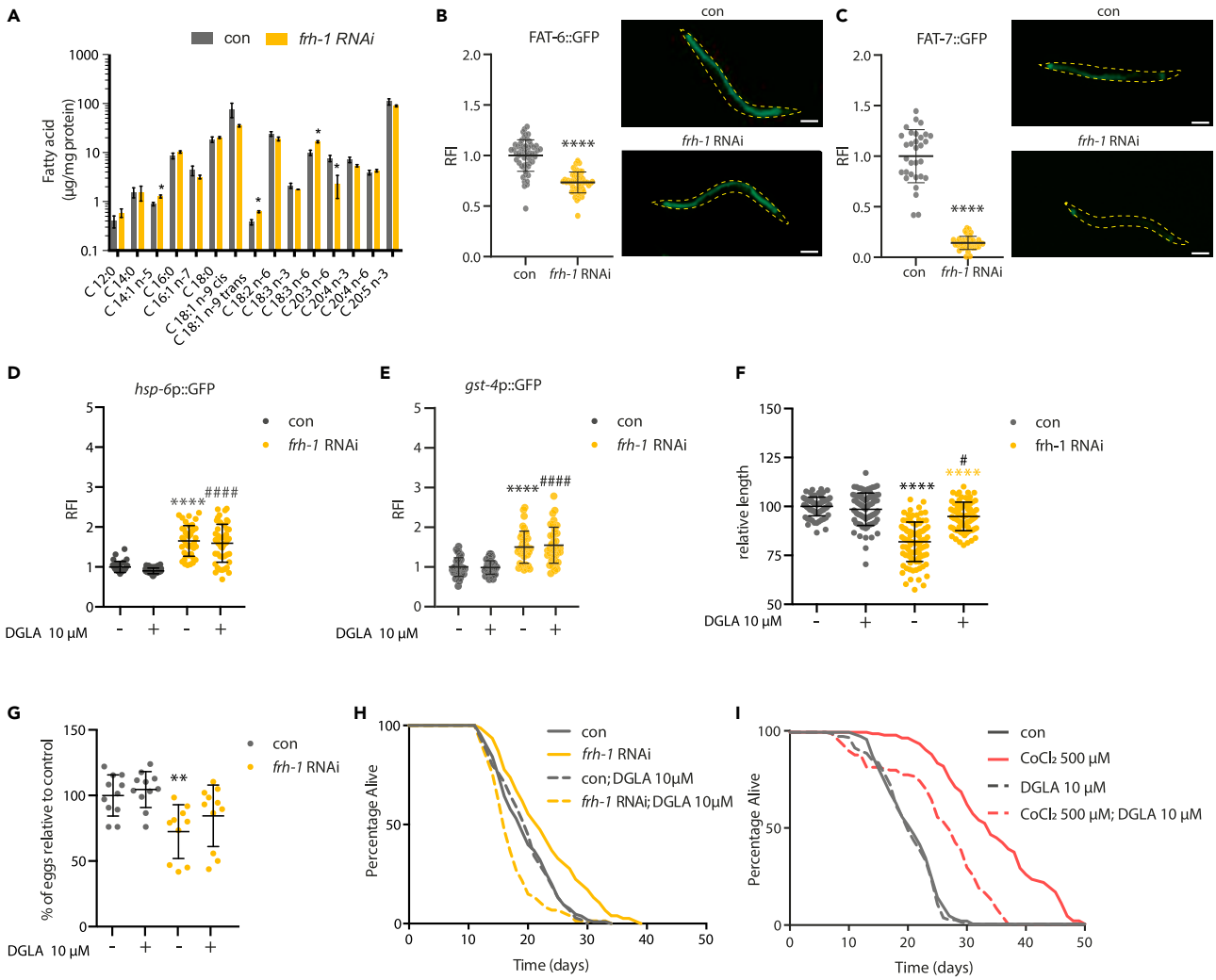

Figure 3. DGLA prevents frataxin silencing extension of lifespan

(A) Quantification of polyunsaturated fatty acid in 4 days old wild-type worms fed bacteria transformed with either empty-vector (con) or vector-expressing dsRNA against *frh-1* (*frh-1* RNAi). Bar graph represent mean ± SEM (n = 3); *p value < 0.05 versus control. Multiple unpaired t-test Holm-Šídák method.

(B and C) Relative fluorescence intensity (RFI) and representative pictures of FAT-7::GFP (B), FAT-6::GFP (C) reporter strains fed as A. Lines in the scatterplot represent means ± SD (n = 3, N = 10–15). ****p value < 0.0001 versus control, unpaired T-test. Scale bar on the representative pictures is 200 µm. Yellow dashed lines represent worm's perimeter.

(D and E) Relative fluorescence intensity (RFI) quantification of *hsp-6*p::GFP (D), *gst-4*p::GFP (C) reporter strains fed as in A and left untreated (–) or treated (+) with Dihomo-γ-linolenic acid (DGLA 10 µM). Lines in the scatterplot represent means ± SD (n = 3, N = 10–15), two-way ANOVA (Tukey's multiple comparison test), ****p value < 0.0001 versus control left untreated, ####p value < 0.0001 versus control treated with DGLA.

(F) Quantification of relative worms' length in 4 days old wild-type animals fed and treated as (D-E). Lines in the scatterplot represent means ± SD (n = 4, N = 15). Black "*" versus control untreated, yellow "*" versus *frh-1* RNAi untreated, ****p value < 0.0001, #p value < 0.05 versus control treated, two-way ANOVA (Tukey's multiple comparison test).

(G) Quantification of number of eggs from 4 days old worms released in 4 h and normalized against the not treated control worms. Animals were fed and treated as in (D-E). Lines in the scatterplot represent means ± SD (n = 3, N = 3–5). **p value < 0.01 versus untreated control, two-way ANOVA (Tukey's multiple comparison test).

(H) Kaplan-Meier survival curves of wild-type strain fed bacteria transformed with either empty-vector (con) or vector-expressing dsRNA against *frh-1* (*frh-1* RNAi) and left untreated or treated with DGLA (DGLA 10 µM). Comparison between curves was done using the log-rank test (Table 1).

(I) Kaplan-Meier survival curves of wild-type strain left untreated (con) or treated with $CoCl_2$ ($CoCl_2$ 500 µM) with or without DGLA (DGLA 10 µM). Comparison between curves was done using the log-rank test (Table 1).

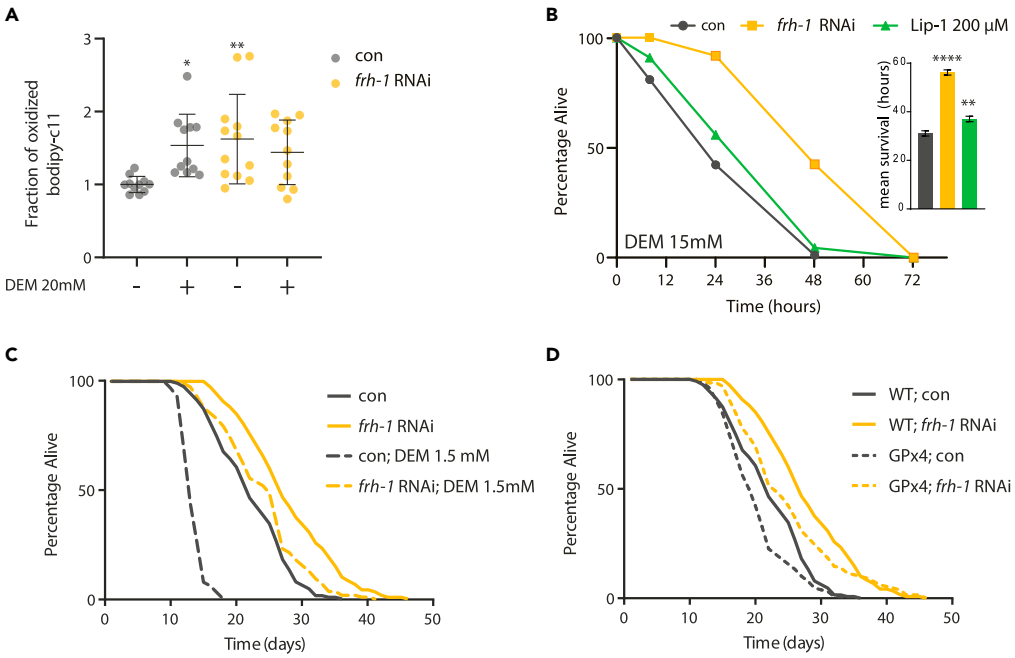

Figure 4. Frataxin depletion extends lifespan via GSH/GPx-dependent and -independent mechanisms

(A) Lipid peroxidation quantified as the amount of oxidized bodipy-C11 in 3 days old-type worms fed bacteria transformed with either empty-vector (con) or vector-expressing dsRNA against *frh-1* (*frh-1* RNAi) and left untreated (−) or treated (+) with diethyl maleate for 6 h (DEM 20 mM). Lines in the scatterplot represent means ± SD (n = 3). *p value < 0.05, two-way ANOVA (Tukey's multiple comparison test).

(B) Survival curves of wild-type worms treated with 15 mM DEM starting from day 5 of adulthood. Worms were fed bacteria transformed with either empty-vector (con) or vector-expressing dsRNA against *frh-1* (*frh-1* RNAi) or treated with liproxstatin (Lip-1 200 µM) starting from L4. The average survival time ±SD for each condition is shown as a bar graph on the right side of the survival curves. Comparison between curves was done using the log-rank test (Table 1). Addionally, mean survival time was tested using one-way ANOVA (Tukey's multiple comparison test), **p value < 0.01, ****p value < 0.0001 versus control.

(C) Kaplan-Meier survival curves of wild-type strain fed bacteria transformed with either empty-vector (con) or vector-expressing dsRNA against *frh-1* (*frh-1* RNAi) and left untreated or treated with 1.5 mM DEM from L4. Comparison between curves was done using the log-rank test (Table 1).

(D) Kaplan-Meier survival curves of wild-type (WT) and GPx4 (GPx4) strains fed bacteria transformed with either empty-vector (con) or vector-expressing dsRNA against *frh-1* (*frh-1* RNAi). Comparison between curves was done using the log-rank test (Table 1).

of GSH and GPx4 depletions were not fully suppressed by *frh-1* silencing indicating GSH/GPx regulated pathways indeed play a role in frataxin-control of lifespan. Data collected so far suggest *frh-1* RNAi promotes lifespan via GSH/GPx(4)-dependent and -independent mechanisms that most likely compensate for the detrimental effects of GSH depletion-induced lipid peroxidation and ferroptosis.

Frataxin depletion impacts on neuroimmune, detoxification, metabolic, and redox regulatory processes across lifespan

To identify new anti-aging mechanisms possibly counteracting the ferroptotic machinery, we then carried out a combined transcriptomic and proteomic analysis upon pro-longevity *frh-1* silencing. Gene expression analysis displayed a great reproducibility within the samples and a striking separation between wild-type and frataxin depleted animals during aging (4,7,14 days old, Figure 5A). Cluster analysis of age-dependent changes in gene expression in wild-type animals (Figure S4) showed that roughly half of the genes had a net upregulation (3817) while half were downregulated (4308) during aging. Downregulated clusters, as expected, are enriched in genes involved in cell cycle and reproduction (cluster 1, 899 genes), mitochondria and metabolic activities especially regulating carbon, amino acids, nucleotide, and glucose metabolism (cluster 7, 496 genes), as well as in genes regulating cellular differentiation, developmental, transcriptional, and biosynthetic processes (cluster 8, 425 genes). Not surprisingly, these clusters decrease during aging

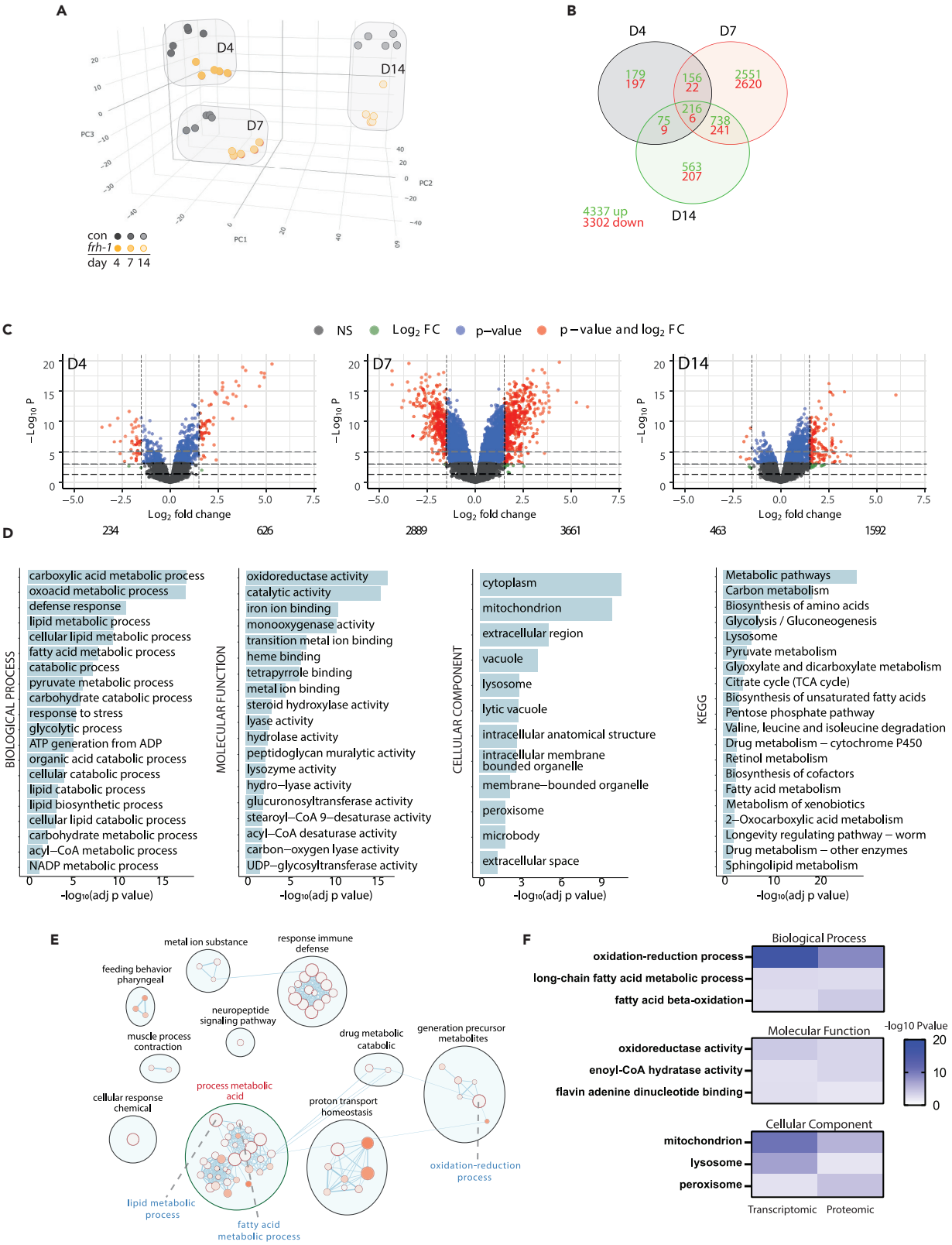
A
D4
D14
D7
PC1
PC2
PC3
con
frh-1
day 4 7 14
B
D4
D7
D14
179
197
156
22
2551
2620
216
6
75
9
738
241
563
207
4337 up
3302 down
C
NS
Log2 FC
p−value
p−value and log2 FC
D4
D7
D14
−Log10 P
Log2 fold change
234
626
2889
3661
463
1592
D
BIOLOGICAL PROCESS
carboxylic acid metabolic process
oxoacid metabolic process
defense response
lipid metabolic process
cellular lipid metabolic process
fatty acid metabolic process
catabolic process
pyruvate metabolic process
carbohydrate catabolic process
response to stress
glycolytic process
ATP generation from ADP
organic acid catabolic process
cellular catabolic process
lipid catabolic process
lipid biosynthetic process
cellular lipid catabolic process
carbohydrate metabolic process
acyl−CoA metabolic process
NADP metabolic process
-log10(adj p value)
MOLECULAR FUNCTION
oxidoreductase activity
catalytic activity
iron ion binding
monooxygenase activity
transition metal ion binding
heme binding
tetrapyrrole binding
metal ion binding
steroid hydroxylase activity
lyase activity
hydrolase activity
peptidoglycan muralytic activity
lysozyme activity
hydro−lyase activity
glucuronosyltransferase activity
stearoyl−CoA 9−desaturase activity
acyl−CoA desaturase activity
carbon−oxygen lyase activity
UDP−glycosyltransferase activity
-log10(adj p value)
CELLULAR COMPONENT
cytoplasm
mitochondrion
extracellular region
vacuole
lysosome
lytic vacuole
intracellular anatomical structure
intracellular membrane bounded organelle
membrane−bounded organelle
peroxisome
microbody
extracellular space
-log10(adj p value)
KEGG
Metabolic pathways
Carbon metabolism
Biosynthesis of amino acids
Glycolysis / Gluconeogenesis
Lysosome
Pyruvate metabolism
Glyoxylate and dicarboxylate metabolism
Citrate cycle (TCA cycle)
Biosynthesis of unsaturated fatty acids
Pentose phosphate pathway
Valine, leucine and isoleucine degradation
Drug metabolism − cytochrome P450
Retinol metabolism
Biosynthesis of cofactors
Fatty acid metabolism
Metabolism of xenobiotics
2−Oxocarboxylic acid metabolism
Longevity regulating pathway − worm
Drug metabolism − other enzymes
Sphingolipid metabolism
-log10(adj p value)
E
metal ion substance
response immune defense
feeding behavior pharyngeal
neuropeptide signaling pathway
muscle process contraction
drug metabolic catabolic
generation precursor metabolites
cellular response chemical
process metabolic acid
proton transport homeostasis
oxidation−reduction process
lipid metabolic process
fatty acid metabolic process
F
Biological Process
oxidation-reduction process
long-chain fatty acid metabolic process
fatty acid beta-oxidation
Molecular Function
oxidoreductase activity
enoyl-CoA hydratase activity
flavin adenine dinucleotide binding
-log10 Pvalue
20
10
0
Cellular Component
mitochondrion
lysosome
peroxisome
Transcriptomic
Proteomic

Figure 5. Frataxin depletion impacts on neuroimmune, detoxification, metabolic, and redox regulatory processes across lifespan

(A) Wild-type worms fed bacteria transformed with either empty-vector (con) or vector-expressing dsRNA against *frh-1* (*frh-1*) were collected for gene and protein expression analysis at 4, 7, and 14 days of age. Principal component analysis plot based on the normalized microarray expression matrix. Each circle represents one microarray sample, and the colors correspond to the treatment as indicated in the figure legend. The same microarray time points are highlighted with a light-gray balloon (n = 5).

(B) Venn diagram showing differentially expressed genes (DEG) between wild-type worms fed bacteria transformed with either empty-vector or vector-expressing dsRNA against *frh-1*. The number of unique and common DEG (FC $\geq$ 1.5 and with a Padj $\leq$ 0.05) are dived in up-(green) and down-regulated(red) and grouped according to the respective time points, 4 days (D4), 7 days (D), and 14 days (D14).

(C) Volcano plots of normalized microarray expression matrix showing the gene expression values for worms fed with dsRNA against *frh-1* relative to empty vector and collected at different time point, 4 days (D4), 7 days (D), and 14 days (D14).

(D) Gene ontology and KEGG analysis plots of the differentially expressed genes across lifespan (3-,7-,14-days-old worms).

(E) Enrichment map created using the enrichment map plugin in cystoscape with the following parameters: q-value < 0.05 and edge-cut-off 0.4. The gene-set was created in https://biit.cs.ut.ee/gprofiler/gost using the differentially expressed genes over time as in D.

(F) GO comparison between the transcriptomic and proteomic differentially expressed genes and proteins across lifespan (3-,7-,14-days-old worms). The heatmap shows the -log10(p value) of enrichment test for each comparison.

with different trajectories; genes belonging to cluster 1 (cell cycle) mainly decrease after day 7; genes belonging to cluster 7 (carboxylic metabolic processes) linearly decrease from 4 to 14 days; while genes belonging to cluster 8 (system development) display the strongest drop between 4 and 7 days. Instead, surprisingly, two clusters with a small fraction of genes primarily involved in the regulation of neuronal differentiation, development, morphogenesis, neurotransmission (cluster 2, 193 genes and cluster 3, 161 genes) had a slightly net upregulation throughout lifespan. Moreover, other two small clusters (cluster 5, 223 genes and cluster 6, 173 genes) containing mainly genes regulating stress response against pathogens and insults were strongly (cluster 5) or mildly (cluster 6) induced between 4 and 7 days and then slightly reduced with the net results of being upregulated (cluster 5) or downregulated (cluster 6) at 14 days old. Finally, two big clusters displayed the highest upregulation with continuous increase through lifespan: the biggest cluster (cluster 4, 984 genes) contains all genes involved in response to stress, pathogens and insults, with many genes belonging kinases signaling (especially MAPK); while the last cluster (cluster 9, 441 genes) contains a variety of genes involved in cell-cell communication processes *e.g.,* secretion, transport, exocytosis, cell junctions, and synapses.

A total of 7639 genes (4337 up and 3302 down) were instead differentially expressed between age-synchronized populations of wild-type and long-lived *frh-1*-depleted animals (Figures 5B and 5C). Perhaps not surprisingly given the role of frataxin in mitochondrial functions, the expression of genes regulating mitochondrial activities, carbon and lipid metabolism and redox homeostasis were significantly changed by *frh-1* depletion (Figures 5D and 5E). A closer look to clusters of the differentially expressed genes throughout animals' lifespan (Figure S5), revealed that processes involved in small molecules homeostasis (e.g., metabolites, ions, iron, NAD precursors), neuropeptide and synaptic functions, as well as defense mechanisms are also significantly affected by *frh-1* depletion. These changes are in agreement with previous studies indicating a role for mitochondria-regulated molecules,[8,47,48] neurons[49,50] and detoxification responses[51,51,52] in mitochondrial-stress extension of *C. elegans* lifespan.

When coupled to the changes in animals' proteome at the same ages, what primarily stood out in our analysis are redox and lipid homeostasis regulatory processes (Figure 5F; Figure S6A), key players in the regulation of ferroptosis. The gene and protein expression profiles are in agreement with the lipidomic analysis with *fat-6* and *fat-7* expression also being reduced at gene level (Figures 6A and 6B). Of note, most of the same processes affected across lifespan are already modulated when comparing the results in 4-day-old animals (Figure S6B), when the frail period has not yet started. This indicates early changes in gene/protein expression are induced early in life in frataxin depleted animals and maintained throughout life to promote longevity. Most importantly, our analysis revealed a vast number of redox and lipid regulatory genes modulated by pro-longevity *frh-1* RNAi (Figure 6C), suggesting novel potential anti-aging mechanisms that may act by counteracting ferroptosis (graphical abstract).

DISCUSSION

Our work provides evidence that limiting iron availability, via genetic (*frh-1* silencing) or chemical (BP) interventions, delays aging and protects against hypoxia-, age-, and proteotoxicity-induced neuromuscular damage and functional decline. Moreover, we identify inhibition of ferroptosis as a possible molecular mechanism mediating the beneficial effects of *frh-1* silencing, clearly suggesting a common mechanistic

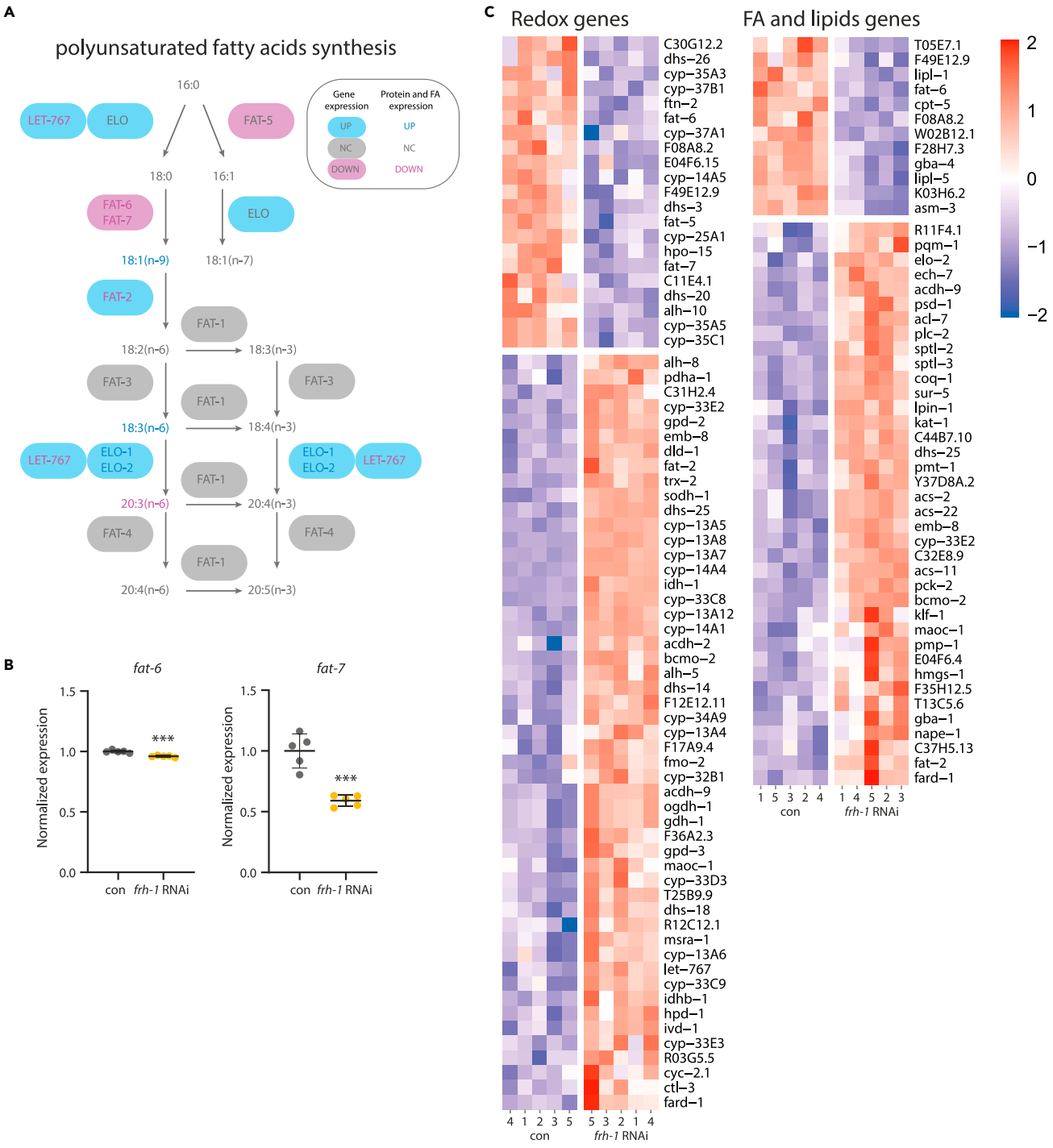

Figure 6. Frataxin depletion impacts on lipids and redox regulatory processes already in young animals

(A) Schematic representation of polyunsaturated fatty acids synthesis pathway summarizing genes, proteins, and fatty acids changes induced by frataxin silencing in wild-type 4 days old animals. Light blue color indicates upregulation, purple downregulation, and gray indicates no modulation.

(B) Scatterplot of *fat-6* and *fat-7* genes normalized expression from day 4 of microarray analysis of worms fed with dsRNA against *frh-1* (*frh-1* RNAi) relative to worms fed with empty vector (con). ***p value < 0.001 versus con unpaired t-test, lines in the scatterplot represent means ± SD (n = 5). (Adjusted p value from the microarray analysis are < 0.05 for *fat-6* and < 0.0001 for *fat-7*).

(C) Heatmaps of genes (from day 4 of microarray) enriched in selected and aggregated gene ontology terms for Redox related processes and fatty acid (FA) and lipid regulatory terms. Aggregated redox GO terms are: GO:0016491, GO:0016705, GO:0016712, GO:0016717, GO:0016620, and GO:0016903. Aggregate FA and lipid GO terms are: GO:0006631, GO:0044242, GO:0016042, and GO:0006629.

determinant for treatments limiting iron availability. These finding have important repercussion in light of the emerging role of ferroptosis in the pathogenesis of different NDD.[53,54] Indeed, the beneficial effects of mild oxygen depletion (or HP) or of mild mitochondria stress (mitohormesis) have been shown and suggested as potential therapeutic strategies.[55–60] However, it is not trivial to fine-tune oxygen levels or mitochondrial activity to trigger beneficial effects without surpassing the critical threshold leading to detrimental consequences. The bottleneck in the exploitation of these preconditioning approaches as therapeutic interventions in fact relies on the low feasibility of their practical application. The identification of more finely tunable interventions mimicking hypoxia or mitochondria preconditioning, such as iron chelators already used in the clinic or undergoing clinical trials,[61,61–63] or of modulators of downstream molecular players (e.g., GSH, FA) mediating their beneficial effects, may thus suggest more feasible preventive or therapeutic approaches to interfere with neuropathological processes.

HP has known beneficial effects against severe hypoxia-induced neuromuscular damage across species,[18] and we show here that mild mitochondrial stress (via *frh-1* silencing) and iron depletion (via the iron chelator BP) may similarly provide protection against neuromuscular degeneration induced by hypoxia, aging, or accumulation of proteotoxic proteins. It is worth noting that the beneficial effect of the iron chelator is dose dependent, and, similar to mitochondria stress,[59,64] it is elicited only when the interventions are applied at sub-lethal doses already during animal development. This clearly indicates that the metabolic remodeling associated with mitohormesis and iron depletion must occur early in life to promote protection against aging and age-associated features.[65]

Different phenotypic features are concurrently associated with the pro-longevity effect induced by mitochondria stress such as reduced animals' size and egg-lay rate, prolonged fertility period, and delay neuromuscular functional decline during aging.[49,59] Interestingly, while decline in *C. elegans* motility is often regarded as a health-related parameter, our data suggest that rather than locomotion activity, pharyngeal pumping is a very sensitive parameter affected by severe hypoxia and ameliorated by the different pro-longevity interventions. This is remarkable considering that *C. elegans* pharynx is considered an ancestral mammalian heart, sharing genetic regulation with hearth embryonic development and recapitulating its electrophysiological properties, pointing to convergent evolution between two autonomous muscular pumps.[66] Of note, pharyngeal pumping is often used as sensitive readout for age-modulating interventions, as well as to monitor neuromuscular (including heart)-associated pathologies.[67–70]

In search of common molecular mechanisms mediating the beneficial effects of iron-depleting interventions, we sought to investigate whether ferroptosis may play a role. Indeed, ferroptosis is a form of GSH-regulated non-apoptotic cell death mediated by iron-induced lipid (PUFA) peroxidation[20] and our work indicate frataxin depletion impact on different key ferroptosis players. Namely, *frh-1* RNAi in *C. elegans* increases the pool of reduced GSH and decreases iron ROS and lipid content,[8,34] all factors which can clearly concur to limit ferroptosis cell death. Our data strongly point toward regulation of lipid metabolic processes modulated by frataxin to suppress ferroptosis. Most notably, DGLA a central ferroptosis mediator[71] suppresses lifespan extension induced by frataxin and CoCl2 and *frh-1* RNAi prevented DEM-induced lipid peroxidation. However, we also found that *frh-1* RNAi in basal condition increased lipid peroxidation revealed by oxidation of the FA analog BODIPY, but did not increase the production of MDA, an end-product of lipid peroxidation. These discrepancies may be ascribed to technical differences in the sensitivity and reproducibility of the two assays.[44] If one considers the TBARS assay as being less sensitive,[44] the increased lipid peroxidation induced by *frh-1* RNAi in basal conditions revealed by BODIPY, clearly resemble a typical hormetic effect. Moreover, it is still possible that frataxin regulation of FA metabolism impacts on ferroptosis via alternative routes. Yet, interestingly, the intrinsic differences of the two assays i.e., one revealing the initial step (oxidation) the other measuring a final product (MDA) of lipid peroxidation, may in fact also disclose real biological effects modulated by frataxin silencing.

We have previously shown that *frh-1* RNAi significantly reduces animals' lipid content, which could be ascribed to reduced lipid droplets formation/accumulation. Interestingly, a decreased content of lipid droplets has been shown to protect against ferroptosis.[72] Moreover, we found frataxin depletion activates *hlh-30*/TFEB, a central mediator of lipid metabolism and of autophagy and different evidence indicates that molecular components of the autophagic process regulate ferroptotic cell death.[73,74] Of note, similar to the bimodal effects on lifespan elicited by mitochondrial hormesis and iron depletion,[8,59,75] also the GSH conjugating agent used in our study (DEM) was shown to influence *C. elegans* lifespan in a non-linear

response.[43] Moreover, according to a beneficial role of GSH-regulated pathways, loss of GSH-redox balance induces proteotoxicity by inhibiting autophagy in *C. elegans* NDD models.[76] We showed in the past that *frh-1* silencing in *C. elegans* not only impacts GSH levels but also increases autophagy, which is casually involved in the specification of frataxin-depleted animals' longevity.[34] It will be thus very interesting to establish whether reduced iron availability and lipid remodeling impact ferroptosis through the same or parallel mechanisms and whether a crosstalk between the autophagy and ferroptosis machinery actually plays a role in regulating health span upon iron and/or frataxin depletion.

Furthermore, although GPx4 quadruple mutant partially suppresses frataxin silencing extension of lifespan, our data suggest ferroptosis suppression by frataxin depletion likely occurs via the induction of compensatory GPx4-independent pathway, which remain to be identified. Two enzymes suppressing ferroptosis have been originally described, namely GSH-reductase-4 (GPX4) and CoQ-regulated migration inhibitory factor (MIF).[41,77,78] More recently, dihydroorotate dehydrogenase (DHODH)[79] and G3P-depdentent dehydrogenase 2 (GPD2)[80] were also implicated in ferroptosis suppression, and the list of players regulating this non-apoptotic form of cell death is expected to grow as clearly indicated by the number of publications on ferroptosis (PubMed search in the title) raising from 900, from its discovery to 2020, to 2800 between 2021 and 2022. In *C. elegans* gpx other than GPx4 or other enzymes may therefore, overcome the loss of the four depleted *gpx*-genes and yet to be disclosed enzymes may concur in regulating ferroptosis upon pro-longevity mitochondrial stress. In this direction our combined transcriptomic and proteomic analysis may help to shed light on the temporal dynamic of aging regulation. Our initial analysis pointed toward a central role for redox reaction activities and lipid homeostasis, two processes critically involved in ferroptosis. Interestingly, these processes are already affected early in life (4-days-old animals), further indicating metabolic remodeling must occur during development to promote health span.[64,65] Additional bioinformatic analysis, such as identification of shared regulatory elements or temporal expression patterns in the transcriptomic/proteomic signature, will be required to fully exploit the potential of our omics approach and uncover new genes and signaling modulating aging in wild-type and in response to mitochondrial stress.

Of note, different redox-regulatory genes are suggested by the transcriptomic profile, and it will be interesting to investigate their role in frataxin regulated ferroptosis and more generally in iron depletion- and mitochondrial stress-promoted health effects. Indeed, while the observed beneficial effect of limiting ferroptosis may be specifically ascribed to frataxin depletion, it is still possible that this is a more general effect of reducing iron availability (via mitochondrial hormesis or downstream regulatory pathways). As ferroptosis is emerging as an important mechanism that concur to the pathogenesis of different age-associated neurodegenerative disorders such as Parkinson or Alzheimer disorders,[33,53,54] identification of strategies to counteract ferroptosis may be relevant to fight a variety of NDD. One paradigmatic example is represented by FRDA, ascribed to severe deficiency of frataxin. Reduced oxygen levels were indeed show to ameliorate detrimental outcomes in different FRDA diseases models including the developmental arrest in a *C. elegans frh-1* knockout strain via a compensatory induction of ISC-proteins.[81] Moreover, we observed that in the poly-Q compromised background, *frh-1* RNAi is protective only within two generations, the second being long lived yet sterile. This clearly implies a threshold effect typical of a neuronal hormetic paradigm induced by mild mitochondrial stress.[49] Accordingly, we also observed a basal increase in α-synuclein aggregates induced by *frh-1* RNAi in young animals. The beneficial endpoints on health and lifespan induced by *frh-1* RNAi clearly implies the activation of downstream molecular players that help compensating for the primary genetic defect (*frh-1* suppression), as well as counteracting additional genetic (protein aggregation) or environmental (age, hypoxia) stressors. Our data suggest that additional mechanisms, likely GPx4-independent redox-dependent reactions, may also help counteracting FRDA and more generally different mitochondrio- or neuronal-pathologies. Interestingly, activation of the redox transcription factor Nrf2 prevents ferroptosis in mammalian FRDA models,[82] and we have shown in the past that pro-longevity *frh-1* silencing in *C. elegans* activates the Nrf2 homolog, *skn-1*, and overcome the short lifespan of the *skn-1* depleted animals.[75] Nrf2 may be also activated by hypoxia and hypoxia mimetics like $CoCl_2$[83,84] and can in turn regulate ferroptosis thus, possibly impacting different NDD.[85] Our omics analysis will help identifying additional redox regulatory genes modulated in response to sub-lethal frataxin deficiency, which may then in turn point toward targeted therapeutic approaches for FRDA and possibly other mitochondriopathies or NDD. This may especially be true for genes, which will be found to regulate ferroptosis. Indeed, while cells from frataxin knock-in/knock-out mouse display different hallmarks of ferroptosis (e.g., increased lipid peroxidation and reduced GPx4 expression), they are less sensitive to cell death

induced by GSH depletion upon buthionine sulfoximine treatment[86] clearly indicating frataxin depleted cells induce compensatory genes, which may help counteracting ferroptosis cell death.

In conclusion, frataxin depletion limits different critical ferroptosis player, and we thus suggest inhibition of ferroptosis (via GPx-independent signaling, yet to be identified) as a new possible mechanism induced by mild mitochondrial stress to promote health span, opening the door to novel potential preventive and therapeutic strategies for age-associated NDD.

Limitations of the study

Severe vs mild depletion of different mitochondrial electron transport chain (ETC) regulatory subunits, including *frh-1*, has opposite outcomes on *C. elegans* health span. This mitohormetic effect resembles that observed upon different degrees of oxygen deprivation, and we describe a similar dual effect also for different degrees of iron depletion. Limiting iron availability clearly dampens ferroptosis. We have previously shown that *frh-1* silencing promotes lifespan via iron-depletion and now provide evidence that it also impacts other key ferroptosis players. Based on previous studies revealing similar health span outcomes upon suppression of different ETC regulatory subunits, we assumed here that the anti-ferroptotic role observed with *frh-1* RNAi can be more generally achieved with mild suppression of the ETC. However, this hypothesis requires further investigation (e.g., using pharmacological or genetic suppression of different ETC components), and we cannot currently exclude that the observed protection against ferroptosis is specific of mild frataxin depletion rather than a general effect promoted by mild mitochondrial stress.

STAR★METHODS

Detailed methods are provided in the online version of this paper and include the following:

- KEY RESOURCES TABLE
- RESOURCE AVAILABILITY
  - Lead contact
  - Material availability
  - Data and code availability
- EXPERIMENTAL MODEL AND SUBJECT DETAILS
  - *C. elegans* strains and culture conditions
- METHOD DETAILS
  - RNA-mediated interference (RNAi)
  - Chemical treatments
  - Hypoxia treatment
  - Life span
  - Body bends
  - Pharyngeal pumping
  - Fecundity
  - Quantification of polyQ aggregates
  - Quantification of α-synuclein aggregates
  - Quantification of neuromuscular damage (axonal-beading and muscle nuclei fragmentation)
  - Quantification of GFP-transgene expression by fluorescence microscopy
  - Quantification of lipid peroxidation
  - RNA and proteins extraction for -omics analysis
  - Proteomic analysis
  - Transcriptomic analysis
  - Lipidomic analysis

SUPPLEMENTAL INFORMATION

Supplemental information can be found online at https://doi.org/10.1016/j.isci.2023.106448.

ACKNOWLEDGMENTS

This work was possible thanks to financial support to NV from: the German Research Foundation (DFG grants VE366/3-1; VE366/8-1), the Federal Ministry of Education and Research (JPI-HDHL, Grant no.

01EA1602) and the Heinrich Heine University of Duesseldorf (Start-up grant from the Research Commission of the Medical Faculty). We also thank the Caenorhabditis Genetics Center (funded by the National Institutes of Health Office of Research Infrastructure Programs: P40OD010440), as well as the National Bioresource Project (NBRP) for *C. elegans* strains. We thank the Proteomics Core Facility, Department of Biosciences, University of Oslo for performing the mass spectrometry-based proteomic analyses; this facility is a member of the National Network of Advanced Proteomics Infrastructure (NAPI), which is funded by the Research Council of Norway INFRASTRUKTUR-program (project number: 295910). A fellowship from the European Cooperation in Science and Technology (e-COST BM1408-180116-070017) covered Alfonso Schiavi's visit to Hilde Nilsen Laboratory.

AUTHORS CONTRIBUTIONS

N.V. conceived, supervised, and financially supported the study. A.Sc., E.S.,V.B., and A.Sh. carried out the experiments. N.V. and A.Sc. analyzed the data and wrote the manuscript. S.K., S.N., R.M., and H.N. help analyzing the different—omics data. S.N., R.M., and H.N. provided some reagents and support for the study. All authors discussed the results, edited, commented, and approved manuscript.

DECLARATION OF INTERESTS

The authors declare no competing interests.

INCLUSION AND DIVERSITY

We support inclusive, diverse, and equitable conduct of research.

Received: March 2, 2022
Revised: November 28, 2022
Accepted: March 15, 2023
Published: March 21, 2023

REFERENCES

1. Gell, D.A. (2018). Structure and function of haemoglobins. Blood Cells Mol. Dis. *70*, 13–42. https://doi.org/10.1016/j.bcmd.2017.10.006.

2. Puig, S., Ramos-Alonso, L., Romero, A.M., and Martínez-Pastor, M.T. (2017). The elemental role of iron in DNA synthesis and repair. Metallomics *9*, 1483–1500. https://doi.org/10.1039/c7mt00116a.

3. Papa, S., Martino, P.L., Capitanio, G., Gaballo, A., De Rasmo, D., Signorile, A., and Petruzzella, V. (2012). The oxidative phosphorylation system in mammalian mitochondria. Adv. Exp. Med. Biol. *942*, 3–37. https://doi.org/10.1007/978-94-007-2869-1_1.

4. Jiang, X., Stockwell, B.R., and Conrad, M. (2021). Ferroptosis: mechanisms, biology and role in disease. Nat. Rev. Mol. Cell Biol. *22*, 266–282. https://doi.org/10.1038/s41580-020-00324-8.

5. Schiavi, A., Strappazzon, F., and Ventura, N. (2020). Mitophagy and iron: two actors sharing the stage in age-associated neuronal pathologies. Mech. Ageing Dev. *188*, 111252. https://doi.org/10.1016/j.mad.2020.111252.

6. DeLoughery, T.G. (2017). Iron deficiency anemia. Med. Clin. North Am. *101*, 319–332. https://doi.org/10.1016/j.mcna.2016.09.004.

7. Pivina, L., Semenova, Y., Doşa, M.D., Dauletyarova, M., and Bjørklund, G. (2019). Iron deficiency, cognitive functions, and neurobehavioral disorders in children. J. Mol. Neurosci. *68*, 1–10. https://doi.org/10.1007/s12031-019-01276-1.

8. Schiavi, A., Maglioni, S., Palikaras, K., Shaik, A., Strappazzon, F., Brinkmann, V., Torgovnick, A., Castelein, N., De Henau, S., Braeckman, B.P., et al. (2015). Iron-starvation-induced mitophagy mediates lifespan extension upon mitochondrial stress in C. elegans. Curr. Biol. *25*, 1810–1822. https://doi.org/10.1016/j.cub.2015.05.059.

9. Lee, D.W., Andersen, J.K., and Kaur, D. (2006). Iron dysregulation and neurodegeneration: the molecular connection. Mol. Interv. *6*, 89–97. https://doi.org/10.1124/mi.6.2.6.

10. Gourley, B.L., Parker, S.B., Jones, B.J., Zumbrennen, K.B., and Leibold, E.A. (2003). Cytosolic aconitase and ferritin are regulated by iron in Caenorhabditis elegans. J. Biol. Chem. *278*, 3227–3234. https://doi.org/10.1074/jbc.M210333200.

11. López-Otín, C., Blasco, M.A., Partridge, L., Serrano, M., and Kroemer, G. (2013). The hallmarks of aging. Cell *153*, 1194–1217. https://doi.org/10.1016/j.cell.2013.05.039.

12. Falk, M.J. (2021). The pursuit of precision mitochondrial medicine: harnessing preclinical cellular and animal models to optimize mitochondrial disease therapeutic discovery. J. Inherit. Metab. Dis. *44*, 312–324. https://doi.org/10.1002/jimd.12319.

13. Anzovino, A., Lane, D.J.R., Huang, M.L.H., and Richardson, D.R. (2014). Fixing frataxin: 'ironing out' the metabolic defect in Friedreich's ataxia. Br. J. Pharmacol. *171*, 2174–2190. https://doi.org/10.1111/bph.12470.

14. Ventura, N., Rea, S., Henderson, S.T., Condo, I., Johnson, T.E., and Testi, R. (2005). Reduced expression of frataxin extends the life span of Caenorhabditis elegans. Aging Cell *4*, 109–112. ACE149 [pii]. https://doi.org/10.1111/j.1474-9726.2005.00149.x.

15. Puccio, H., Simon, D., Cossée, M., Criqui-Filipe, P., Tiziano, F., Melki, J., Hindelang, C., Matyas, R., Rustin, P., and Koenig, M. (2001). Mouse models for Friedreich ataxia exhibit cardiomyopathy, sensory nerve defect and Fe-S enzyme deficiency followed by intramitochondrial iron deposits. Nat. Genet. *27*, 181–186. https://doi.org/10.1038/84818.

16. Rodriguez, M., Snoek, L.B., De Bono, M., and Kammenga, J.E. (2013). Worms under stress: C. elegans stress response and its relevance to complex human disease and aging. Trends Genet. *29*, 367–374. https://doi.org/10.1016/j.tig.2013.01.010.

17. Lee, J.W., Ko, J., Ju, C., and Eltzschig, H.K. (2019). Hypoxia signaling in human diseases and therapeutic targets. Exp. Mol. Med. *51*,

1–13. https://doi.org/10.1038/s12276-019-0235-1.

18. Dasgupta, N., Patel, A.M., Scott, B.A., and Crowder, C.M. (2007). Hypoxic preconditioning requires the apoptosis protein CED-4 in C. elegans. Curr. Biol. *17*, 1954–1959. https://doi.org/10.1016/j.cub.2007.10.017.

19. Liu, J., Gu, Y., Guo, M., and Ji, X. (2021). Neuroprotective effects and mechanisms of ischemic/hypoxic preconditioning on neurological diseases. CNS Neurosci. Ther. *27*, 869–882. https://doi.org/10.1111/cns.13642.

20. Dixon, S.J., Lemberg, K.M., Lamprecht, M.R., Skouta, R., Zaitsev, E.M., Gleason, C.E., Patel, D.N., Bauer, A.J., Cantley, A.M., Yang, W.S., et al. (2012). Ferroptosis: an iron-dependent form of nonapoptotic cell death. Cell *149*, 1060–1072. https://doi.org/10.1016/j.cell.2012.03.042.

21. Wenger, R.H. (2002). Cellular adaptation to hypoxia: O2-sensing protein hydroxylases, hypoxia-inducible transcription factors, and O2-regulated gene expression. FASEB J *16*, 1151–1162. https://doi.org/10.1096/fj.01-0944rev.

22. Powell-Coffman, J.A. (2010). Hypoxia signaling and resistance in C. elegans. Trends Endocrinol. Metab. *21*, 435–440. https://doi.org/10.1016/j.tem.2010.02.006.

23. Goldberg, M.A., Dunning, S.P., and Bunn, H.F. (1988). Regulation of the erythropoietin gene: evidence that the oxygen sensor is a heme protein. Science *242*, 1412–1415. https://doi.org/10.1126/science.2849206.

24. Lee, D.W., and Andersen, J.K. (2006). Role of HIF-1 in iron regulation: potential therapeutic strategy for neurodegenerative disorders. Curr. Mol. Med. *6*, 883–893. https://doi.org/10.2174/156652406779010849.

25. Caldwell, K.A., Willicott, C.W., and Caldwell, G.A. (2020). Modeling neurodegeneration in Caenorhabditis elegans. Dis. Model. Mech. *13*, dmm046110. https://doi.org/10.1242/dmm.046110.

26. Liang, J.J.H., McKinnon, I.A., and Rankin, C.H. (2020). The contribution of C. elegans neurogenetics to understanding neurodegenerative diseases. J. Neurogenet. *34*, 527–548. https://doi.org/10.1080/01677063.2020.1803302.

27. Alexander, A.G., Marfil, V., and Li, C. (2014). Use of Caenorhabditis elegans as a model to study Alzheimer's disease and other neurodegenerative diseases. Front. Genet. *5*, 279. https://doi.org/10.3389/fgene.2014.00279.

28. Fawcett, E.M., Hoyt, J.M., Johnson, J.K., and Miller, D.L. (2015). Hypoxia disrupts proteostasis in Caenorhabditis elegans. Aging Cell *14*, 92–101. https://doi.org/10.1111/acel.12301.

29. Link, C.D. (2006). C. elegans models of age-associated neurodegenerative diseases: lessons from transgenic worm models of Alzheimer's disease. Exp. Gerontol. *41*, 1007–1013. https://doi.org/10.1016/j.exger.2006.06.059.

30. McColl, G., Roberts, B.R., Pukala, T.L., Kenche, V.B., Roberts, C.M., Link, C.D., Ryan, T.M., Masters, C.L., Barnham, K.J., Bush, A.I., and Cherny, R.A. (2012). Utility of an improved model of amyloid-beta (Abeta(1)(-)(4)(2)) toxicity in Caenorhabditis elegans for drug screening for Alzheimer's disease. Mol. Neurodegener. *7*, 57. https://doi.org/10.1186/1750-1326-7-57.

31. Perez, M.A., Magtanong, L., Dixon, S.J., and Watts, J.L. (2020). Dietary lipids induce ferroptosis in caenorhabditiselegans and human cancer cells. Dev. Cell *54*, 447–454.e4. https://doi.org/10.1016/j.devcel.2020.06.019.

32. Yao, M.Y., Liu, T., Zhang, L., Wang, M.J., Yang, Y., and Gao, J. (2021). Role of ferroptosis in neurological diseases. Neurosci. Lett. *747*, 135614. https://doi.org/10.1016/j.neulet.2020.135614.

33. Weiland, A., Wang, Y., Wu, W., Lan, X., Han, X., Li, Q., and Wang, J. (2019). Ferroptosis and its role in diverse brain diseases. Mol. Neurobiol. *56*, 4880–4893. https://doi.org/10.1007/s12035-018-1403-3.

34. Schiavi, A., Torgovnick, A., Kell, A., Megalou, E., Castelein, N., Guccini, I., Marzocchella, L., Gelino, S., Hansen, M., Malisan, F., et al. (2013). Autophagy induction extends life span and reduces lipid content in response to frataxin silencing in C. elegans. Exp. Gerontol. *48*, 191–201. https://doi.org/10.1016/j.exger.2012.12.002.

35. O'Rourke, E.J., Kuballa, P., Xavier, R., and Ruvkun, G. (2013). omega-6 Polyunsaturated fatty acids extend life span through the activation of autophagy. Genes Dev. *27*, 429–440. https://doi.org/10.1101/gad.205294.112.

36. Ma, D.K., Rothe, M., Zheng, S., Bhatla, N., Pender, C.L., Menzel, R., and Horvitz, H.R. (2013). Cytochrome P450 drives a HIF-regulated behavioral response to reoxygenation by C. elegans. Science *341*, 554–558. https://doi.org/10.1126/science.1235753.

37. Schiavi, A., Runci, A., Maiorino, T., Naso, F.D., Barenys, M., Fritsche, E., Strappazzon, F., and Ventura, N. (2022). Cobalt chloride has beneficial effects across species through a hormetic mechanism. Front. Cell Dev. Biol. *10*, 986835. https://doi.org/10.3389/fcell.2022.986835.

38. Yang, W.S., and Stockwell, B.R. (2016). Ferroptosis: death by lipid peroxidation. Trends Cell Biol. *26*, 165–176. https://doi.org/10.1016/j.tcb.2015.10.014.

39. Zheng, J., and Conrad, M. (2020). The metabolic underpinnings of ferroptosis. Cell Metab. *32*, 920–937. https://doi.org/10.1016/j.cmet.2020.10.011.

40. Friedmann Angeli, J.P., Schneider, M., Proneth, B., Tyurina, Y.Y., Tyurin, V.A., Hammond, V.J., Herbach, N., Aichler, M., Walch, A., Eggenhofer, E., et al. (2014). Inactivation of the ferroptosis regulator Gpx4 triggers acute renal failure in mice. Nat. Cell Biol. *16*, 1180–1191. https://doi.org/10.1038/ncb3064.

41. Yang, W.S., SriRamaratnam, R., Welsch, M.E., Shimada, K., Skouta, R., Viswanathan, V.S., Cheah, J.H., Clemons, P.A., Shamji, A.F., Clish, C.B., et al. (2014). Regulation of ferroptotic cancer cell death by GPX4. Cell *156*, 317–331. https://doi.org/10.1016/j.cell.2013.12.010.

42. Jenkins, N.L., James, S.A., Salim, A., Sumardy, F., Speed, T.P., Conrad, M., Richardson, D.R., Bush, A.I., and McColl, G. (2020). Changes in ferrous iron and glutathione promote ferroptosis and frailty in aging Caenorhabditis elegans. Elife *9*, e56580. https://doi.org/10.7554/eLife.56580.

43. Urban, N., Tsitsipatis, D., Hausig, F., Kreuzer, K., Erler, K., Stein, V., Ristow, M., Steinbrenner, H., and Klotz, L.O. (2017). Non-linear impact of glutathione depletion on C. elegans life span and stress resistance. Redox Biol. *11*, 502–515. https://doi.org/10.1016/j.redox.2016.12.003.

44. Domínguez-Rebolledo, Á.E., Martínez-Pastor, F., Fernández-Santos, M.R., del Olmo, E., Bisbal, A., Ros-Santaella, J.L., and Garde, J.J. (2010). Comparison of the TBARS assay and BODIPY C11 probes for assessing lipid peroxidation in red deer spermatozoa. Reproduction in domestic animals = Zuchthygiene *45*, e360–e368. https://doi.org/10.1111/j.1439-0531.2009.01578.x.

45. He, F., Huang, X., Wei, G., Lin, X., Zhang, W., Zhuang, W., He, W., Zhan, T., Hu, H., and Yang, H. (2022). Regulation of ACSL4-catalyzed lipid peroxidation process resists cisplatin ototoxicity. Oxid. Med. Cell. Longev. *2022*, 3080263. https://doi.org/10.1155/2022/3080263.

46. Sakamoto, T., Maebayashi, K., Nakagawa, Y., and Imai, H. (2014). Deletion of the four phospholipid hydroperoxide glutathione peroxidase genes accelerates aging in Caenorhabditis elegans. Gene Cell. *19*, 778–792. https://doi.org/10.1111/gtc.12175.

47. Mishur, R.J., Khan, M., Munkácsy, E., Sharma, L., Bokov, A., Beam, H., Radetskaya, O., Borror, M., Lane, R., Bai, Y., and Rea, S.L. (2016). Mitochondrial metabolites extend life span. Aging Cell *15*, 336–348. https://doi.org/10.1111/acel.12439.

48. Bradshaw, P.C. (2019). Cytoplasmic and mitochondrial NADPH-coupled redox systems in the regulation of aging. Nutrients *11*. https://doi.org/10.3390/nu11030504.

49. Maglioni, S., Schiavi, A., Runci, A., Shaik, A., and Ventura, N. (2014). Mitochondrial stress extends life span in C. elegans through neuronal hormesis. Exp. Gerontol. *56*, 89–98. https://doi.org/10.1016/j.exger.2014.03.026.

50. Durieux, J., Wolff, S., and Dillin, A. (2011). The cell-non-autonomous nature of electron transport chain-mediated longevity. Cell *144*, 79–91. https://doi.org/10.1016/j.cell.2010.12.016.

51. Herholz, M., Cepeda, E., Baumann, L., Kukat, A., Hermeling, J., Maciej, S., Szczepanowska, K., Pavlenko, V., Frommolt, P., and Trifunovic,

A. (2019). KLF-1 orchestrates a xenobiotic detoxification program essential for longevity of mitochondrial mutants. Nat. Commun. *10*, 3323. https://doi.org/10.1038/s41467-019-11275-w.

52. Mao, K., Ji, F., Breen, P., Sewell, A., Han, M., Sadreyev, R., and Ruvkun, G. (2019). Mitochondrial dysfunction in C. elegans activates mitochondrial relocalization and nuclear hormone receptor-dependent detoxification genes. Cell Metab. *29*, 1182–1191.e4. https://doi.org/10.1016/j.cmet.2019.01.022.

53. Jakaria, M., Belaidi, A.A., Bush, A.I., and Ayton, S. (2021). Ferroptosis as a mechanism of neurodegeneration in Alzheimer's disease. J. Neurochem. *159*, 804–825. https://doi.org/10.1111/jnc.15519.

54. Vitalakumar, D., Sharma, A., and Flora, S.J.S. (2021). Ferroptosis: a potential therapeutic target for neurodegenerative diseases. J. Biochem. Mol. Toxicol. *35*, e22830. https://doi.org/10.1002/jbt.22830.

55. Gohel, D., and Singh, R. (2021). Mitohormesis; Potential implications in neurodegenerative diseases. Mitochondrion *56*, 40–46. https://doi.org/10.1016/j.mito.2020.11.011.

56. Musci, R.V., Hamilton, K.L., and Linden, M.A. (2019). Exercise-induced mitohormesis for the maintenance of skeletal muscle and healthspan extension. Sports (Basel) *7*, 170. https://doi.org/10.3390/sports7070170.

57. Caricati-Neto, A., Errante, P.R., and Menezes-Rodrigues, F.S. (2019). Recent advances in pharmacological and non-pharmacological strategies of cardioprotection. Int. J. Mol. Sci. *20*, 4002. https://doi.org/10.3390/ijms20164002.

58. Li, S., Hafeez, A., Noorulla, F., Geng, X., Shao, G., Ren, C., Lu, G., Zhao, H., Ding, Y., and Ji, X. (2017). Preconditioning in neuroprotection: from hypoxia to ischemia. Prog. Neurobiol. *157*, 79–91. https://doi.org/10.1016/j.pneurobio.2017.01.001.

59. Rea, S.L., Ventura, N., and Johnson, T.E. (2007). Relationship between mitochondrial electron transport chain dysfunction, development, and life extension in Caenorhabditis elegans. PLoS Biol. *5*, 2599–e306. PLBI-RA-2325 [pii]. https://doi.org/10.1371/journal.pbio.0050259.

60. Merry, T.L., and Ristow, M. (2016). Mitohormesis in exercise training. Free Radic. Biol. Med. *98*, 123–130. https://doi.org/10.1016/j.freeradbiomed.2015.11.032.

61. Reddy, P.S., Locke, M., and Badawy, S.M. (2022). A systematic review of adherence to iron chelation therapy among children and adolescents with thalassemia. Ann. Med. *54*, 326–342. https://doi.org/10.1080/07853890.2022.2028894.

62. Yang, S., Zhang, M.C., Leong, R., Mbuagbaw, L., Crowther, M., and Li, A. (2022). Iron chelation therapy in patients with low- to intermediate-risk myelodysplastic syndrome: a systematic review and meta-analysis. Br. J. Haematol. *197*, e9–e11. https://doi.org/10.1111/bjh.17998.

63. Wijesinghe, T.P., Dharmasivam, M., Dai, C.C., and Richardson, D.R. (2021). Innovative therapies for neuroblastoma: the surprisingly potent role of iron chelation in up-regulating metastasis and tumor suppressors and down-regulating the key oncogene, N-myc. Pharmacol. Res. *173*, 105889. https://doi.org/10.1016/j.phrs.2021.105889.

64. Dillin, A., Hsu, A.L., Arantes-Oliveira, N., Lehrer-Graiwer, J., Hsin, H., Fraser, A.G., Kamath, R.S., Ahringer, J., and Kenyon, C. (2002). Rates of behavior and aging specified by mitochondrial function during development. Science *298*, 2398–2401.

65. Maglioni, S., Mello, D.F., Schiavi, A., Meyer, J.N., and Ventura, N. (2019). Mitochondrial bioenergetic changes during development as an indicator of C. elegans health-span. Aging (Albany NY) *11*, 6535–6554. https://doi.org/10.18632/aging.102208.

66. Mango, S. (2007). The C. elegans pharynx: a model for organogenesis. WormBook, 1–26. https://doi.org/10.1895/wormbook.1.129.1.

67. Diomede, L., Romeo, M., Rognoni, P., Beeg, M., Foray, C., Ghibaudi, E., Palladini, G., Cherny, R.A., Verga, L., Capello, G.L., et al. (2017). Cardiac light chain amyloidosis: the role of metal ions in oxidative stress and mitochondrial damage. Antioxid. Redox Signal. *27*, 567–582. https://doi.org/10.1089/ars.2016.6848.

68. Wellenberg, A., Brinkmann, V., Bornhorst, J., Ventura, N., Honnen, S., and Fritz, G. (2021). Cisplatin-induced neurotoxicity involves the disruption of serotonergic neurotransmission. Pharmacol. Res. *174*, 105921. https://doi.org/10.1016/j.phrs.2021.105921.

69. Eckers, A., Jakob, S., Heiss, C., Haarmann-Stemmann, T., Goy, C., Brinkmann, V., Cortese-Krott, M.M., Sansone, R., Esser, C., Ale-Agha, N., et al. (2016). The aryl hydrocarbon receptor promotes aging phenotypes across species. Sci. Rep. *6*, 19618. https://doi.org/10.1038/srep19618.

70. Maglioni, S., Schiavi, A., Melcher, M., Brinkmann, V., Luo, Z., Laromaine, A., Raimundo, N., Meyer, J.N., Distelmaier, F., and Ventura, N. (2022). Neuroligin-mediated neurodevelopmental defects are induced by mitochondrial dysfunction and prevented by lutein in C. elegans. Nat. Commun. *13*, 2620. https://doi.org/10.1038/s41467-022-29972-4.

71. Yang, W.S., Kim, K.J., Gaschler, M.M., Patel, M., Shchepinov, M.S., and Stockwell, B.R. (2016). Peroxidation of polyunsaturated fatty acids by lipoxygenases drives ferroptosis. Proc. Natl. Acad. Sci. USA *113*, E4966–E4975. https://doi.org/10.1073/pnas.1603244113.

72. Chen, X., Kang, R., Kroemer, G., and Tang, D. (2021). Organelle-specific regulation of ferroptosis. Cell Death Differ. *28*, 2843–2856. https://doi.org/10.1038/s41418-021-00859-z.

73. Zhou, B., Liu, J., Kang, R., Klionsky, D.J., Kroemer, G., and Tang, D. (2020). Ferroptosis is a type of autophagy-dependent cell death. Semin. Cancer Biol. *66*, 89–100. https://doi.org/10.1016/j.semcancer.2019.03.002.

74. Sun, Y., Berleth, N., Wu, W., Schlütermann, D., Deitersen, J., Stuhldreier, F., Berning, L., Friedrich, A., Akgün, S., Mendiburo, M.J., et al. (2021). Fin56-induced ferroptosis is supported by autophagy-mediated GPX4 degradation and functions synergistically with mTOR inhibition to kill bladder cancer cells. Cell Death Dis. *12*, 1028. https://doi.org/10.1038/s41419-021-04306-2.

75. Ventura, N., Rea, S.L., Schiavi, A., Torgovnick, A., Testi, R., and Johnson, T.E. (2009). p53/CEP-1 increases or decreases life span, depending on level of mitochondrial bioenergetic stress. Aging Cell *8*, 380–393. [pii]. https://doi.org/10.1111/j.1474-9726.2009.00482.x ACE482.

76. Guerrero-Gómez, D., Mora-Lorca, J.A., Sáenz-Narciso, B., Naranjo-Galindo, F.J., Muñoz-Lobato, F., Parrado-Fernández, C., Goikolea, J., Cedazo-Minguez, Á., Link, C.D., Neri, C., et al. (2019). Loss of glutathione redox homeostasis impairs proteostasis by inhibiting autophagy-dependent protein degradation. Cell Death Differ. *26*, 1545–1565. https://doi.org/10.1038/s41418-018-0270-9.

77. Bersuker, K., Hendricks, J.M., Li, Z., Magtanong, L., Ford, B., Tang, P.H., Roberts, M.A., Tong, B., Maimone, T.J., Zoncu, R., et al. (2019). The CoQ oxidoreductase FSP1 acts parallel to GPX4 to inhibit ferroptosis. Nature *575*, 688–692. https://doi.org/10.1038/s41586-019-1705-2.

78. Ingold, I., Berndt, C., Schmitt, S., Doll, S., Poschmann, G., Buday, K., Roveri, A., Peng, X., Porto Freitas, F., Seibt, T., et al. (2018). Selenium utilization by GPX4 is required to prevent hydroperoxide-induced ferroptosis. Cell *172*, 409–422.e21. https://doi.org/10.1016/j.cell.2017.11.048.

79. Mao, C., Liu, X., Zhang, Y., Lei, G., Yan, Y., Lee, H., Koppula, P., Wu, S., Zhuang, L., Fang, B., et al. (2021). DHODH-mediated ferroptosis defence is a targetable vulnerability in cancer. Nature *593*, 586–590. https://doi.org/10.1038/s41586-021-03539-7.

80. Wu, S., Mao, C., Kondiparthi, L., Poyurovsky, M.V., Olszewski, K., and Gan, B. (2022). A ferroptosis defense mechanism mediated by glycerol-3-phosphate dehydrogenase 2 in mitochondria. Proc. Natl. Acad. Sci. USA *119*. e2121987119. https://doi.org/10.1073/pnas.2121987119.

81. Ast, T., Meisel, J.D., Patra, S., Wang, H., Grange, R.M.H., Kim, S.H., Calvo, S.E., Orefice, L.L., Nagashima, F., Ichinose, F., et al. (2019). Hypoxia rescues frataxin loss by restoring iron sulfur cluster biogenesis. Cell *177*, 1507–1521.e16. https://doi.org/10.1016/j.cell.2019.03.045.

82. La Rosa, P., Petrillo, S., Turchi, R., Berardinelli, F., Schirinzi, T., Vasco, G., Lettieri-Barbato, D., Fiorenza, M.T., Bertini, E.S., Aquilano, K., and Piemonte, F. (2021). The Nrf2 induction prevents ferroptosis in Friedreich's Ataxia. Redox Biol. *38*, 101791. https://doi.org/10.1016/j.redox.2020.101791.

83. Huang, B.W., Miyazawa, M., and Tsuji, Y. (2014). Distinct regulatory mechanisms of the human ferritin gene by hypoxia and hypoxia

mimetic cobalt chloride at the transcriptional and post-transcriptional levels. Cell. Signal. *26*, 2702–2709. https://doi.org/10.1016/j.cellsig.2014.08.018.

84. Kalpana, S., Dhananjay, S., Anju, B., Lilly, G., and Sai Ram, M. (2008). Cobalt chloride attenuates hypobaric hypoxia induced vascular leakage in rat brain: molecular mechanisms of action of cobalt chloride. Toxicol. Appl. Pharmacol. *231*, 354–363. https://doi.org/10.1016/j.taap.2008.05.008.

85. Song, X., and Long, D. (2020). Nrf2 and ferroptosis: a new research direction for neurodegenerative diseases. Front. Neurosci. *14*, 267. https://doi.org/10.3389/fnins.2020.00267.

86. Turchi, R., Tortolici, F., Guidobaldi, G., Iacovelli, F., Falconi, M., Rufini, S., Faraonio, R., Casagrande, V., Federici, M., De Angelis, L., et al. (2020). Frataxin deficiency induces lipid accumulation and affects thermogenesis in brown adipose tissue. Cell Death Dis. *11*, 51. https://doi.org/10.1038/s41419-020-2253-2.

87. Perez-Riverol, Y., Bai, J., Bandla, C., García-Seisdedos, D., Hewapathirana, S., Kamatchinathan, S., Kundu, D.J., Prakash, A., Frericks-Zipper, A., Eisenacher, M., et al. (2022). The PRIDE database resources in 2022: a hub for mass spectrometry-based proteomics evidences. Nucleic Acids Res. *50*, D543–D552. https://doi.org/10.1093/nar/gkab1038.

88. Deline, M.L., Vrablik, T.L., and Watts, J.L. (2013). Dietary supplementation of polyunsaturated fatty acids in Caenorhabditis elegans. J. Vis. Exp. https://doi.org/10.3791/50879.

89. Torgovnick, A., Schiavi, A., Shaik, A., Kassahun, H., Maglioni, S., Rea, S.L., Johnson, T.E., Reinhardt, H.C., Honnen, S., Schumacher, B., et al. (2018). BRCA1 and BARD1 mediate apoptotic resistance but not longevity upon mitochondrial stress in Caenorhabditis elegans. EMBO Rep. *19*, e45856. https://doi.org/10.15252/embr.201845856.

90. Han, S.K., Lee, D., Lee, H., Kim, D., Son, H.G., Yang, J.S., Lee, S.J.V., and Kim, S. (2016). Oasis 2: online application for survival analysis 2 with features for the analysis of maximal life span and health span in aging research. Oncotarget *7*, 56147–56152. https://doi.org/10.18632/oncotarget.11269.

91. Schindelin, J., Arganda-Carreras, I., Frise, E., Kaynig, V., Longair, M., Pietzsch, T., Preibisch, S., Rueden, C., Saalfeld, S., Schmid, B., et al. (2012). Fiji: an open-source platform for biological-image analysis. Nat. Methods *9*, 676–682. https://doi.org/10.1038/nmeth.2019.

92. Zhou, Y., Falck, J.R., Rothe, M., Schunck, W.H., and Menzel, R. (2015). Role of CYP eicosanoids in the regulation of pharyngeal pumping and food uptake in Caenorhabditis elegans. J. Lipid Res. *56*, 2110–2123. https://doi.org/10.1194/jlr.M061887.

STAR★METHODS

KEY RESOURCES TABLE

REAGENT or RESOURCE	SOURCE	IDENTIFIER
Bacterial and virus strains		
*E. coli*OP50	CGC	WB Cat# WBStrain00041969
E. coli RNAi feeding strain L4440 HT115(DE3)	source bioscience	WB Cat# WBStrain00041079
*E. coli frh-1*IV RNAi in HT115(DE3) background	doi:10.1016/j.exger.2012.12.002	N/A
Chemicals, peptides, and recombinant proteins		
cOmplete™, EDTA-free Protease Inhibitor Cocktail	Roche	Cat# 04693132001
Cobalt(II)-Chlorid Hexahydrat	Sigma-Aldrich Chemie GmbH	Cat# C8661
Tergitol	Sigma-Aldrich Chemie GmbH	Cat# NP40S
2,2′ dipyridyl	Carl Roth	Cat# 4153
DGLA	Cayman Chemical Company	Cat# 90230
LA	Cayman Chemical Company	Cat# 90150
Liproxstatin	Gentaur GmbH	Cat# B4987
Diethyl maleate	Sigma-Aldrich Chemie GmbH	Cat# D97703
DMSO	Carl Roth	Cat# A994
BODIPY-C11	Cayman Chemical Company	Cat# 27086
RIPA Buffer	Millipore	Cat# 20-188
QIAshredder	Qiagen	Cat# 79654
Critical commercial assays		
TBARS (TCA Method) Assay Kit	Cayman Chemical Company	Cat# 700870
RNeasy Mini Kit	Qiagen	Cat# 74104
Deposited data		
Microarray data deposited into NCBI Gene Expression Omnibus	This paper	GSE225776
The mass spectrometry proteomics data have been deposited to the ProteomeXchange Consortium	This paper	PXD040724
Experimental models: Organisms/strains		
C. elegans: Strain N2	CGC	WB Cat# WBStrain00000001
C. elegans: Strain AM141 rmIs133 [*unc-54p*::Q40::YFP]X	CGC	WB Cat# WBStrain00000183
C. elegans: Strain NL5901 pkIs2386 [*unc-54*p::alphasynuclein::YFP + *unc-119*(+)]	CGC	WB Cat# WBStrain00029035
C. elegans: Strain GMC101 dvIs100 [*unc-54p*::A-beta-1-42::*unc-54* 3′-UTR + *mtl-2p*::GFP]	CGC	WB Cat# WBStrain00007866
C. elegans: Strain SK4005 zdIs5 [*mec-4*::GFP + *lin-15*(+)]	CGC	WB Cat# WBStrain00034088
C. elegans: Strain UA49 [baInl2; *unc-54p*::α-syn::GFP, *rol-6* (*su1006*)]	The University of Alabama; Tuscaloosa AL, United States of America; Department of Biological Sciences (Guy Caldwell)	WB Cat# WBStrain00035182
C. elegans: Strain CL2166 vIs19 [(pAF15)gst-4p::GFP::NLS] III	CGC	WB Cat# WBStrain00005102

(*Continued on next page*)

Continued

REAGENT or RESOURCE	SOURCE	IDENTIFIER
C. elegans: Strain SJ4100 zcls13 [*hsp-6p*::GFP + *lin-15*(+)]	CGC	WB Cat# WBStrain00034068
C. elegans: Strain BX113 waEx15 [*fat-7*::GFP + lin15(+)]	CGC	WB Cat# WBStrain00004017
C. elegans: Strain BX115 waEx16 [*fat-6*::GFP + *lin15*(+)]	CGC	WB Cat# WBStrain00004018
C. elegans: Strain KJP2 *gpx-1(tm2100)I*; *gpx-2(tm2895)II*; *gpx-6(tm2525)IV*; *gpx-7(ksu1)X*	School of Pharmacy, Kitasato University, 5-9-1 Shirokane, Minato-ku, Tokyo, 108-8641, Japan (Taro Sakamoto)	N/A
Software and algorithms		
GraphPad Prism 9.0	GraphPad Prism Software, Inc	https://www.graphpad.com/
R	R Foundation	https://www.r-project.org/
Rstudio IDE Open Source Edition	Posit Software	https://posit.co/products/open-source/rstudio/
R package: arrayQualityMetrics	*Bioconductor*	https://doi.org/10.18129/B9.bioc.arrayQualityMetrics
R package: EnhancedVolcano	*Bioconductor*	https://doi.org/10.18129/B9.bioc.EnhancedVolcano
R package: Oligo	*Bioconductor*	https://doi.org/10.18129/B9.bioc.oligo
R package: gprofiler2	The R Foundation	https://cran.r-project.org/web/packages/gprofiler2/index.html
R package: ViSEAGO	*Bioconductor*	https://doi.org/10.18129/B9.bioc.ViSEAGO
R package: Limma	*Bioconductor*	https://doi.org/10.18129/B9.bioc.limma
Scaf-fold	Proteome Software	https://www.proteomesoftware.com/
Cytoscape	Cytoscape Consortium	https://cytoscape.org/
Enrichment Map	Cytoscape Consortium	https://www.baderlab.org/Software/EnrichmentMap
OASIS 2	Structural Bioinformatics Lab https://sbi.postech.ac.kr/	https://sbi.postech.ac.kr/oasis2/surv/
ImageJ	Image Processing and Analysis in Java	http://ImageJ.nih.gov/ij/

RESOURCE AVAILABILITY

Lead contact

Further information and requests for resources and reagents should be directed to and will be fulfilled by the lead contact, Natascia Ventura (natascia.ventura@uni-duesseldorf.de).

Material availability

This study did not generate any new reagents.

Data and code availability

- Microarray data have been deposited at GEO while the mass spectrometry proteomics data have been deposited to the ProteomeXchange Consortium via the PRIDE,[87] and data are publicly available as of the date of publication. Accession numbers are listed in the key resources table.
- This paper does not report original code
- Any additional information required to reanalyze the data reported in this paper is available from the lead contact upon request.

EXPERIMENTAL MODEL AND SUBJECT DETAILS

C. elegans strains and culture conditions

The following strains were used in this study: N2 wild type, AM141: rmIs133 [*unc-54p*:Q40:YFP], NL5901: pkIs2386 [*unc-54p*:α-syn:gfp:YFP + *unc-119*(+)], SK4005: zdIs5[*mec-4p*:GFP], UA49: [baInl2; *unc-54p*:α-syn:GFP, rol-6 (su1006)], CL2166: dvIs19[pAF15(*gst-4*:GFP:NLS)], SJ4100: zcIs13[*hsp-6p*:GFP], BX113: *lin-15*B&*lin-15*A(n765)X; waEx15 [*fat-7*:GFP + *lin15*(+)], BX115: *lin-15*B&*lin-15*A(n765)X; waEx16 [*fat-6*:GFP + lin15(+)], KJP2: *gpx-1*(*tm2100*)I; *gpx-2*(*tm2895*)II; *gpx-6*(*tm2535*)IV; *gpx-7*(*ksu1*)X; GMC101 dvIs100 *[unc-54p*:A-beta-1-42::*unc-54* 3′-UTR + *mtl-2p*:GFP].

All strains were maintained and kept synchronized by egg lay at 20°C on Nematode Growth Media (NGM) agar supplemented with *Escherichia coli* (OP50 or transformed HT115), unless otherwise indicated.

METHOD DETAILS

RNA-mediated interference (RNAi)

Genes of interest were silenced by feeding *E. coli* HT115(DE3) expressing plasmids transformed with *frh-1* dsRNA.[14] Worms were treated with RNAi expressing bacteria from eggs until the end of the experiment.

Chemical treatments

Cobalt chloride (CoCl2 C8661, Sigma Aldrich), was dissolved at 0.1 M stock solution in ddH_2O, sterilized using a 0.22 μM filter and supplemented to the NGM after autoclaving at the concentration of interest.

2,2′ dipyridyl (BP, 4153 Carl Roth) was dissolved in ddH_2O and added to NGM to the indicated concentrations.

Fatty acids were supplied as previously described by others.[88] Briefly, NGM media was supplemented with Tergitol (NP40S Sigma) and dihomo-gamma-linolenic acid (DGLA, 20:3n-6) (90230 Cayman) or linolenic acid (LA, 18:2 n-6) (90150, Cayman) were added at the indicated concentrations. Worms were treated from eggs until the end of the experiments.

Liproxtatin (Lip-1 B4987, Gentaur GmbH) and Diethyl maleate (DEM D97703, Sigma-Aldrich) treatment were carried out as previously described by others.[42] Briefly, Lip-1 was dissolved in DMSO then added to molten NGM (55°C) to a final concentration of 200 μM Lip-1 (0.5% DMSO), worms were transfer on Lip-1 plates as L4/Young Adults.

DEMwas diluted in DMSO then added directly to molten NGM (55°C) to a final concentration of 15 mM DEM (0.5% DMSO) for the survival assay, 1.5 mM DEM (0.5% DMSO) for the life span assay, or to 20 mM (0.5% DMSO) for the lipid peroxidation assay. Plates were seeded with bacteria, dried under a laminar flow hood, and used within 24 h.

For the survival assay, nematodes were transferred on 15 mM DEM plates starting on day 5 of adulthood and survival was scored at 12, 24, 48 and 72 h after treatment.

For the life span assay nematodes were transfer on 1.5 mM plates as L4/Young Adults. Plates containing DMSO 0.5% were used as control. All experiment with DEM were conducted at 20°C.

Hypoxia treatment

Worms were placed into a hypoxia plexiglass chamber (Billups-Rothenberg). The oxygen was exchanged and removed inside the hypoxia chamber by flushing a gas mixture (95% N2, 5% CO2) for 10 min (flux 15 L/min). Then worms were left in the hypoxia chamber for 4 (preconditioning) or 48 h (severe hypoxia) at 26°C.

After the preconditioning treatment worms were allowed to recover at 20°C for 20 h prior further treatment with Hypoxia.

Life span

Survival analysis were carried out with standard procedure in the field as routinely carried out in our laboratory.[89] Briefly, synchronized population of 60–80 worms were used to start the life span analysis. Animals

were transfer on fresh plates every day during the fertile phase and at the end of the fertile period worms were transferred every other day. Animals not able to move upon prodding and with no pharyngeal pumping were scored as dead Animals were scored as not moving when no sinusoid locomotory activity was observed anymore upon prodding. Survival analysis was performed in OASIS 2[90] using the Kaplan Meier estimator. Statistical different were evaluated using the log rank test between the pooled population or worms and p values were adjusted for multiple comparisons by Bonferoni method.

Body bends

The movement of adult worms (3 days after egg-lay) was scored on bacteria-free NGM plates. Worms after transferring were left recover for 50-60 s before starting the counting. Afterward the body bends were counted for 1 min.

Pharyngeal pumping

Pharyngeal pumping was scored using a stereomicroscope (Leica MZ10 F). The pumping of each single adult worms was counted for 1 min and the mean were used for the analysis. Body bends were checked in at least 10 single worms in 3 independent trials for each experimental condition.

Fecundity

The Fecundity of animals was estimated counting the eggs laid in a period of 4 h from 3 worms on 4 different plates in each condition and repeated in 3 independent trials.

Quantification of polyQ aggregates

PolyQ40 aggregates were visualized by fluorescence microscopy (250× magnification) in worms anesthetized with 10 mM sodium azide (Sigma, S2002). The number of the aggregates in the head region was quantified in Fiji.[91]

Quantification of α-synuclein aggregates

α-synuclein aggregates in the head muscles at the indicated age were visualized by fluorescence microscopy (400× magnification) in worms anesthetized with 10 mM sodium azide (Sigma, S2002). The number of aggregates was scored using a threshold mask to segment the aggregates, then the number of aggregates was measured with the embedded Fiji[91] plugin "Analyze Particles" and the setting were kept the same for each set of experiments.

Quantification of neuromuscular damage (axonal-beading and muscle nuclei fragmentation)

Mechanosensory neurons were visualized using the *mec-4p*:GFP strain, image were acquire by fluorescence microscopy (630× magnification). The number of beads per axon were counted and averaged. Muscle nuclei were visualized using a fluorescence microscope (630 magnification) in the *myo-3p*:GFP strain. Fragmented or missing nuclei were scored as damaged.

Quantification of GFP-transgene expression by fluorescence microscopy

The nematodes were placed in a 15 μL S-Basal plus levamisole 10 mM drop on a microscope glass slide, covered with a cover slide and immediately imaged. Pictures were acquired with an Imager2 Zeiss fluorescence microscope, magnification 25-fold. The images were analyzed with the software ImageJ (http://imagej.nih.gov/ij/). The brightfield images were used to generate the mask to select each single worm pictured and consequently for measure the fluorescence in the correspondent fluorescent filter.

Quantification of lipid peroxidation

BODIPY-C11 (no. 27086 Caymann chemical) staining

3-days old worms (70-80) left untreated or treated for 6 h on 20 mM DEM NGM plates, were washed 3 times with M9 and stained with 500 μL of BODIPY-C11 10 μM solution for 30 min. An additional control group was left unstained. Stained and not stained worms were washed 3 times with M9 before measurement. 125 μL of stained and unstained worms were acquired in triplicate with a microplate reader (Tecan Infinite 200 PRO). Oxidized BODIPY-C11 was measured using 488 nm for the excitation and 530 nm for the emission, while the not-oxidized BODIPY-C11 was measured using 568 nm for the excitation and 590 for the emission.

Background fluorescence of not stained worms was subtracted to each sample. Background corrected fluorescence intensity was used to calculate the ratio of oxidized versus non-oxidized BODIPY-C11.

TBARS (TCA method) assay kit (no. 700870 Caymann chemical)

Proteins were extracted from 3-days old worms (around 300-400 worms) left untreated or treated for 6 h on 20 mM DEM NGM plates. Animals were collected and washed 3 times with M9 and 1 time with double-distilled water and immediately snap-frozen in liquid nitrogen and store at −80°C until needed. Worm proteins were extracted by sonication in RIPA buffer (Millipore cat. 20-188) and protease inhibitor cocktail (Roche cat. 04693132001). 25 μg of protein were used to perform the assay as described in the kit manual. Using a Tecan infinite 200 PRO the fluorescence intensities for each sample, and for the Malondialdehyde (MDA) standard provided with the kit, were measured using 530 nm for the excitation and 556 nm for the emission wavelength.

RNA and proteins extraction for -omics analysis

For RNA and protein extraction, nematodes were collected at day 4, 7 and 14 of adulthood from 3 big NGM plates seeded with bacteria expressing empty-vector (pL4440) or vector-expressing dsRNA against *frh-1*. For each time point/condition around 2000 worms were collected for RNA extraction. Worms were transferred daily on fresh plates to avoid starvation and separate the progenies from the population of interest. For each time point, worms were collected into nuclease-free water and frozen at −80°C for further processing. Worms lysates were prepared using the TissueLyser II (Qiagen), briefly 2 stainless-steel beads (6 mm) were added to the wormś pellet containing the lysis buffer 1:1 v/v then 2 cycles of shaking (2 min at 30 Hz) were performed on each samples. Total RNA was extracted using the RNeasy Mini Kit and QIAshredder according to the manufacturer's instructions (Qiagen-74104 and 79654). 5 different biological replicas were used for each condition. For proteins extraction around 4000 worms were collected from 5-6 big NGM plates, time point, feeding and maintenance were done as described for the RNA extraction.

Proteomic analysis

The proteomics raw data was processed through the use of Scaf-fold software (http://www.proteomesoftware.com/). The exclusive unique peptide count data were exported using a "protein threshold identification" of 99.9%, a "peptide threshold identification" of 95% and a "minimum number of peptides" of 4 in order to identified a protein, the data were then normalized over the maximun number of protein identifiable using a value of 1 for the "minimum number of peptides", consequently the normalized data was processed using the open source tool Bioconductor (http://www.bioconductor.org). We compared the different experimental conditions using Limma Package, which allows the use of Empirical Bayesian methods to find the differential expressed gene/proteins between the conditions of interest. Briefly, we estimated the fold changes and standard errors by fitting a linear model for each protein, then we applied empirical Bayes smoothing to the standard errors.

Transcriptomic analysis

The RNA was processed by the Center for Biological and Medical Research (BMFZ), Facility of the Heinrich Heine University of Düsseldorf. cDNA synthesis and quality control, hybridization and Affymetrix *C. elegans* Gene 1.0 ST Microarrays scanning were performed. Obtained raw data (Affymetrix.cel-files) were used for further analysis using R version 4.0.3 (2020-10-10)

First, a quality control of the array was performed using the package arrayQualityMetrics_3.46.0, no single array was excluded from the analysis. The data were normalized using Robust Multiple-array Average (RMA) by the oligo package and annotated using pd.elegene.1.0.st package. The extracted expression matrix was analyzed using the limma package to find the differentially expressed genes (DEGs) (with FDR correction using a cut-off of adjusted p value<0.05.)

The list of unfiltered differentially expressed genes was plotted using the package EnhancedVolcano as volcano plots Statistical enrichment analysis of differentially expressed gene lists was performed using the gprofiler2 (0.2.0) package in R. ViSEAGO (1.4.0) Bioconductor package for clustering biological functions using Gene Ontology and semantic similarity was used to generate the heatmaps.

Lipidomic analysis

For the PUFA and eicosanoid analysis, 4-days olds worms grown on either the empty vector or *frh-1* RNAi for three generations were used. For this, approximately 3,000 worms (con RNAi) or 6,000 worms (*frh-1* RNAi) were collected in ice-cold S-basal on day 4 after egg-lay. After 3 washing steps with ice-cold S-basal, an almost dry worm pellet was obtained by placing the worms on a 10 μm gauze membrane filter. Resulting worm filter cake masses of 84 ± 2 mg were gained for animals raised on con RNAi and 40 ± 8 mg for worms on *frh-1* RNAi, respectively. The collected worm samples were analyzed for the abundance of PUFA and eicosanoids using HPLC-MS/MS as described previously.[92] The service was provided by the Lipidomix GmbH (Berlin, Germany).